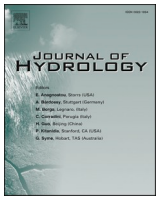
Journal of Hydrology 669 (2026) 135128



Contents lists available at ScienceDirect

Journal of Hydrology

journal homepage: www.elsevier.com/locate/jhydrol



Research papers



A multi-objective simulation-optimisation model for managing saltwater intrusion in a coastal aquifer of the Pacific Island of Vanuatu

Ashneel Sharan [a,b,*], Dilip Kumar Roy [c], Bithin Datta [a], Alvin Lal [d]

[a] Discipline of Civil Engineering, College of Science & Engineering, James Cook University, Townsville, Queensland 4811, Australia
[b] C&R Consulting, Geochemical and Hydrobiological Solutions Pty Ltd, Queensland 4814, Australia
[c] Irrigation and Water Management Division, Bangladesh Agricultural Research Institute, Joydebpur, Gazipur 1701, Bangladesh
[d] Global Centre for Environmental Remediation, College of Engineering, Science and Environment, University of Newcastle, Callaghan, NSW 2308, Australia

ARTICLE INFO

This manuscript was handled by Okke Batelaan, Editor-in-Chief

Keywords:
Saltwater intrusion
SEAWAT
Machine learning
Ensemble surrogate model
Simulation-optimisation
Vanuatu

ABSTRACT

Groundwater resources in Pacific Island countries face threats from climate change, natural disasters, and human activities, with saltwater intrusion (SWI) being a significant issue in coastal aquifers like Vanuatu's Tagabe coastal aquifer. This study developed numerical and machine learning models to manage SWI in the Tagabe aquifer. The SEAWAT was used to create a numerical groundwater model, calibrated and validated with salt concentration data from various monitoring locations (MLs). The model generated input (pumping values) and output (salt concentrations) datasets, which were used to train and test twelve machine learning models or surrogate models. These models were ranked using performance criteria and decision theory, and the top five were used to form ensemble models to predict salt concentrations at four MLs. The Pearson coefficient, Index of Agreement, Kling-Gupta Efficiency and Nash Sutcliffe Efficiency coefficient of four ensemble models at ML1 = 0.745, 0.738, 0.497 and 0.384; ML2 = 0.946, 0.950, 0.753 and 0.848; ML3 = -0.028, 0.166, −0.369 and −0.070; ML4 = 0.415, 0.369, −0.135 and −4.032, respectively. The ensemble models performed better than individual surrogate models, with higher predictive accuracy across different MLs. These models were integrated with the Controlled Elitist Multiple Objective Genetic Algorithm (CEMOGA) to create a simulation-optimisation (S-O) management model, providing Pareto optimal solutions for managing SWI. Verification using the SEAWAT-based numerical model showed that the ensemble models' predictive accuracy was within 7% of the complex numerical model. This study is novel in its use of limited datasets to train twelve machine learning models and the application of ensemble surrogate and S-O management models in Vanuatu, demonstrating their global applicability for managing SWI in coastal aquifers and aiding policymakers in formulating effective groundwater use policies.

1. Introduction

Saltwater intrusion (SWI) is a challenging environmental problem in Pacific Island countries (PIC). The majority of the coastal aquifers in PICs are hydraulically linked with the sea merely because the islands are surrounded by the Pacific Ocean. This hydraulic linkage fuels up SWI rates when the sea level rises, variations in tide heights, and over-abstraction of groundwater resources (Sharan et al. 2021). The management of SWI in PICs is critical predominantly because people mostly use groundwater for their daily needs. The SWI problem needs to be addressed not only in PICs but around the globe.

Different techniques are utilised around the globe in managing SWI rates. Sherif et al. (2014) and Song et al. (2018) proposed rules for water resource usage and minimising SWI by reducing pumping and relocation of production bores. However, this approach is costly and temporary and could affect the water supply and demand ratios. The use of physical sub-surface barriers like cut-off walls and dams is proposed by Abdoulhalik et al. (2017). These physical barriers stop SWI and do not need maintenance. However, the cost of installing physical barriers is immense and time-constrained. On the other hand, the use of hydraulic barriers to control SWI has gained particular attention because it has proved that hydraulic barriers control SWI in coastal aquifers (e.g., Dhar and Datta 2009; Sreekanth and Datta 2011; Roy and Datta 2017a; Lal and Datta 2018).

* Corresponding author at: Discipline of Civil Engineering, College of Science & Engineering, James Cook University, Townsville, Queensland 4811, Australia..
E-mail address: ashneel.sharan@my.jcu.edu.au (A. Sharan).

https://doi.org/10.1016/j.jhydrol.2026.135128
Received 26 June 2024; Received in revised form 9 February 2026; Accepted 10 February 2026
Available online 15 February 2026
0022-1694/© 2026 The Author(s). Published by Elsevier B.V. This is an open access article under the CC BY license (http://creativecommons.org/licenses/by/4.0/).

Dhar and Datta (2009) and Sharan et al. (2023) used hydraulic barriers to manage SWI in coastal aquifers. The authors reported that the use of barrier wells (BWs), injection wells (IWs) and coupled BWs-IWs manages SWI effectively. The authors developed a numerical simulation model and simulated various scenarios, including BW and IW, which managed SWI. However, these hydraulic barriers have some disadvantages, which include the higher BW pumping, availability of freshwater for vertical recharge, and disposal of abstracted brackish or salty water. The method proposed by the authors could be beneficial if the BW pumping could be reduced or minimised and production well (PW) pumping is maximised. Also, reducing salt concentrations without reducing pumping rates from PWs. These are conflicting and multi-objective problems that can only be tackled by linked simulation-optimisation (S-O) modelling techniques (Dhar and Datta 2009).

The S-O methodology utilises a simulation model to replicate aquifer processes and an optimisation model to identify the optimal solution. For instance, to increase the groundwater abstraction rates and reduce salt concentration in coastal aquifers, an optimal groundwater abstraction rate has to be employed using a S-O method. The S-O model would give a set of pumping regimes that would maximise pumping from the production bores and minimise pumping from the barrier wells while controlling saltwater intrusion. This approach is essential for determining the most effective abstraction rates from a set of viable solutions found in the Pareto optimal front. The linkage between simulation and optimisation ensures a comprehensive evaluation, allowing the identification of optimal rates amid various feasible alternatives. S-O has been applied by various researchers in managing SWI (e.g., Bhattacharjya et al. 2007; Dhar and Datta 2009; Roy and Datta 2017). These studies reported that the S-O model successfully provides Pareto optimal front solutions in managing SWI. Other studies on the application of S-O models in groundwater studies are summarised by Sharan et al. (2021).

The first step in developing a linked S-O model is to develop a 3D numerical simulation model. The numerical simulation model plays a crucial role in comprehending and addressing intricate challenges related to the monitoring and management of saltwater intrusion in coastal aquifers. These models accurately depict the groundwater characteristics of the studied region, providing a comprehensive grasp of the inherent physical processes (Lal and Datta 2020). To develop a coupled S-O based saltwater intrusion management model, the simulation model needs to be linked to an optimisation algorithm. However, direct linking of a numerical simulation model with an optimisation algorithm is computationally prohibitive. For instance, to couple the 3D numerical model with an optimisation algorithm (linked S-O), the convergence computational time could take upto months for a single solution (Dhar and Datta 2009).

A method to enhance computational efficiency within a connected S-O approach involves employing reasonably accurate surrogate models. These approximate surrogate models serve as valuable tools for simulating the linked processes of flow and salt transport in coastal aquifers with a high degree of accuracy (Bhattacharjya et al. 2007). These surrogates can substitute the computationally demanding 3D numerical simulation model, leading to enhanced computational efficiency within a connected S-O framework. The repetitive utilisation of these surrogate models by the optimisation algorithm does not impose a substantial computational burden, as these surrogates are simplified renditions of the intricate simulation models (Roy and Datta 2017a).

Some of the machine learning-based surrogate approximators which substituted complex 3D numerical simulation models include genetic programming (Shreekant and Datta, 2011), radial basis function (Papadopoulou et al. 2010), evolutionary polynomial regression (Hussain et al. 2015), support vector machine regression (Lal and Datta 2018), multivariate adaptive regression splines (Roy and Datta, 2017b), Gaussian process regression (Kopsiaftis et al. 2019), Deep Neural Networks (Mo et al. 2020). All the aforementioned prediction artificial intelligence (AI) models are machine learning models. Very few studies have used deep learning models as SWI simulation models. Machine learning models require human interaction, whereas deep learning models learn from the dataset and make their own decisions (Brownlee 2019). Hence, deep learning models may provide accurate results compared to traditional machine learning models (Ahmed et al. 2023). However, deep learning models require immense input–output data sets to give accurate results.

The majority of the studies have used single machine learning models as surrogate approximators in SWI predictions. This study is the first to utilise a large number of machine learning models as surrogate approximators in predicting the SWI of an island aquifer in Vanuatu. The details of all the machine learning models used in this study are given in Section 2 of this paper. This study will also look into the advantages of using ensemble models for SWI predictions. The use of surrogate and ensemble models in predicting SWI in Vanuatu will be applied for the first time. Moreover, this paper will also utilise decision theories to select robust surrogate and ensemble models in predicting SWI. To the best of the author's knowledge, decision theories have not been used to select the best surrogate and ensemble models for SWI prediction in Pacific Island countries (PICs). Furthermore, the other aspects of the significance of this study include the use of Controlled Elitist Multiple Objective Genetic Algorithm (CEMOGA) in optimising the Pareto optimal front solutions. A detailed discussion of multi-objective optimisation algorithms is given in Section 2.3.

The results from this study are of global significance as it builds on the current knowledge of utilising machine learning models in SWI predictions. This study will contribute to the knowledge of which surrogate or ensemble is robust, computer-efficient and accurate in predicting the SWI of a complex and heterogeneous island aquifer. A large number of surrogates and ensembles would also provide a benchmark for the accuracy of SWI predictions in an island coastal aquifer. Another important aspect of this study is that it used a limited number of input–output training patterns to train the surrogate models. This approach saved computational time and provided efficiency in developing the surrogate models. Roy and Datta (2020) and Roy et al. (2024) used 1500 input–output patterns to train the surrogate models. However, the author's computational time was high. Hence, using fewer input–output datasets is one of the novelties of this study. The results will also provide justifications of which decision theories are important in selecting surrogate and ensemble models. Moreover, the results will also highlight the importance of using CEMOGA algorithm in drawing up robust multi-objective SWI management strategies in Vanuatu. The results from this study could be used by policymakers and water engineers in modelling, planning, and decision-making to conserve and utilise the water resources of island aquifers.

2. Methodology

2.1. Study area

The SWI multi-objective management model was developed in this study. A 3D numerical model of Tagabe coastal aquifer, an island aquifer in Vanuatu, was used to develop a multi-objective management model. The study area is shown in Fig. 1.

2.1.1. Country background

Vanuatu, situated east of Australia, consists of 83 islands with diverse landscapes ranging from volcanic mountains to coral atolls. With a population of over 300,000, its capital, Port Vila, is renowned for its natural beauty, attracting tourists for activities like snorkelling, diving, and hiking. Tourism contributes significantly to Vanuatu's economy, comprising 35.5% of its GDP in 2019, alongside agriculture, fishing, and forestry (WTTC 2021). However, Vanuatu faces challenges from natural disasters and climate change impacts, prompting the government to prioritise resilience-building measures (CRCP 2021; VMGD 2023; Sharan 2023).

Vanuatu's six provinces, including Shefa, home to the capital, Efate

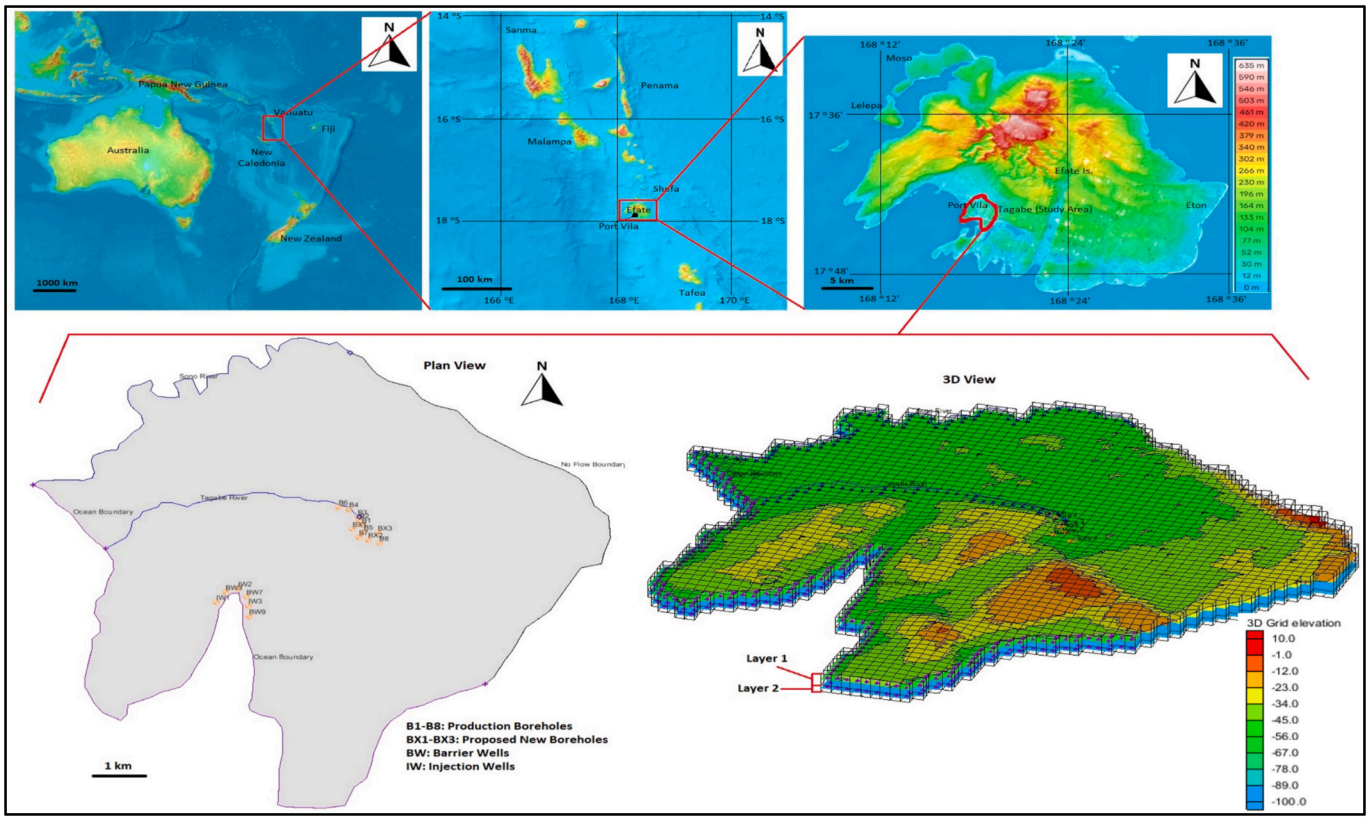


Fig. 1. Study area.).
Source: (Sharan et al. 2024

Island, are characterised by diverse geology shaped by volcanic activity, tectonic movements, and erosion. Efate Island boasts volcanic features like the Yasur volcano and limestone formations formed by marine organisms, along with alluvial deposits from nearby rivers (Bath et al. 1986). Geological processes have shaped the island's topography, with tectonic movements creating faults and folds, and erosion impacting coastal areas due to their low elevation. Despite its geological diversity, Vanuatu's vulnerability to natural disasters underscores the importance of integrating climate adaptation and disaster risk reduction strategies into its development planning to ensure resilience for its people and infrastructure (Sharan et al. 2024).

2.1.2. Site hydrogeology

The water supply for Port Vila, sourced from the Tagabe catchment, faces complex hydrogeological challenges influenced by the island's geology, rainfall patterns, and land use. The catchment comprises a fractured volcanic rock aquifer system primarily composed of basalts and andesites, as reported by the Vanuatu Geohazards Observatory (VGO 2015). Factors affecting groundwater recharge, such as rainfall patterns, land use, and soil characteristics, have been identified by the United Nations Development Programme (UNDP 2016). With Port Vila experiencing rapid urbanisation, population growth, and increased demands from various sectors, including tourism and infrastructure, the freshwater aquifer in Tagabe is under mounting pressure. Climate change exacerbates these challenges, heightening vulnerability and threatening the ability to sustain current and future water needs for Port Vila and Vanuatu as a whole.

The Tagabe catchment features eight active production boreholes supplying water to Port Vila, revealing a hydrogeological profile with two layers, primarily sand and gravel in the upper layer and limestone below. Considering the uncertainties, the limestone layer is conservatively approximated to extend to 20 m below ground level. The Tagabe coastal aquifer, characterised by its heterogeneity, shallowness, and unconfined nature, also receives contributions from two active rivers, Sono and Tagabe, further complicating its dynamics. Covering an area of approximately 57 square kilometres, the aquifer supports multiple boreholes nearby, emphasising the importance of sustainable SWI management strategies to ensure the resilience and longevity of Port Vila's water supply (TRCMP 2018).

2.1.3. Numerical simulation model

The groundwater data provided by the Department of Water Resources, Government of Vanuatu, was limited, comprising bore pumping data from 2017 to 2022 and partial electrical conductivity records from 2019 to 2021. Critical parameters like hydraulic head values and initial concentrations were absent. Despite these limitations, the 3D numerical simulation model was developed utilising the available data to address saltwater intrusion (SWI) management scenarios in the Tagabe coastal aquifer. The boundary conditions and hydrogeological parameters used to develop a 3D groundwater numerical model are given in Table 1.

The numerical 3D groundwater model was developed using flow and transport codes in Groundwater Modelling Systems (GMS) software. SEAWAT was code used in GMS to develop the numerical model. SEAWAT employs a computational framework to simulate three-dimensional groundwater flow in porous materials, accommodating variable density and transient conditions. This is achieved by integrating the functionalities of MODFLOW (develops flow model), which tackles the complexities of variable density flow equations, and MT3DMS (develops transport model), which handles the temporal and spatial aspects of solute transport equations, as outlined by Guo and Langevin (2002).

The conceptual model of the Tagabe coastal aquifer was developed using the MODFLOW-2000 code, encompassing a model domain with dimensions of 7.50 km in the X-direction, 7.61 km in the Y-direction, and 0.1 km in the Z-direction. A 3D finite-difference grid with cell sizes

Table 1
Model parameters and the values used for the model design. .

Definition	Assigned field values	Calibrated values	SI Units
Layer 1 (Sand and gravel)	Hydraulic Conductivity, K = 20 Porosity = 0.35	Hydraulic Conductivity, K = 25.5 Porosity = 0.45	K = m/d Porosity = dimensionless
Layer 2 (Limestone)	Hydraulic Conductivity, K = 35 Porosity = 0.45	Hydraulic Conductivity, K = 40 Porosity = 0.55	
Recharge	0.0004	0.000271	m/d
Horizontal Anisotropy	1		dimensionless
Freshwater Density	1000		kg/m^3
Seawater Density	1025		kg/m^3
Saltwater Concentration	35		kg/m^3
Specific Storage	0.000035		1/m
River conductance	1		m^2/dm
Longitudinal dispersivity	30		m
Density/Con. constant, F	0.7143		dimensionless

Source (Sharan et al. 2024)

of 100 x 100 m was constructed for the entire domain, consisting of two layers with distinct hydraulic conductivities and porosities. Layer 1, extending from 0 to −80 m, had a hydraulic conductivity of 20 m/d and a porosity of 0.35, while layer 2, from −80 to −100 m, exhibited hydraulic conductivity of 35 m/d and porosity of 0.45. Boundary conditions were applied, with the southern boundary designated as a specified head boundary (CHB), the eastern side as a no-flow boundary, and the northwestern boundary representing the Sono River connected to the ocean boundary and no-flow boundary.

Observed hydraulic head values from boreholes in Tagabe were not available, necessitating the assignment of approximate values based on the provided data. CHB values for western and southeastern nodes were set at 9 m and 8.8 m, respectively, maintaining a slight hydraulic gradient towards the landward side. Head values for the Sono River and Tagabe River nodes were also assigned accordingly, with consideration for the presence of salinity in the aquifer, indicating a landward-side hydraulic gradient. Boreholes B1-B8 were incorporated into the model domain along with their specific geographic locations, and transient pumping values from 2017 to 2021 were assigned. Finally, all hydrogeological parameters, boundary conditions, wells, pumping values, and head values were integrated into MODFLOW, and a steady-state simulation spanning 20 years was conducted to establish initial conditions.

SEAWAT was initiated for a 5-year period, utilising pumping data from 2017 to 2021, with calibration based on electrical conductivity (EC) data from boreholes B1, B2, B3, B7, and B8 spanning 2019 to 2020 due to missing data in 2021. EC values were converted to parts per million (ppm) or milligrams/litre (mg/L) and then to kg/m^3. Despite the absence of observed head values, calibration using secondary data was conducted through trial-and-error methods, adjusting initial salt concentrations, recharge values, hydraulic conductivities, and porosities. Following calibration, the model was simulated for the subsequent 20 years (2022–2043), with the calibrated results serving as the base case for the study. The calibrated model was further employed to get the input (pumping) and output (salt concentrations) at four monitoring locations.

2.1.4. Input-output patterns

The calibrated model was used to generate input–output patterns. The decision space was used to generate random pumping values. Decision space consisted of the simulation period (five years), eight production bores and six barrier wells. These decision space values gave seventy variables, where fourteen (total wells) were multiplied by the simulation period. Once the number of variables was fixed, then the number of simulations was set as 200. Hence, the quasi-random sequences for all wells were generated 200 times using the data range between lower bound (0 m^3/d) and upper bound (1200 m^3/d). Once the decision space was defined and set, the pumping values (input patterns) were randomly generated using the Halton sequence in MATLAB (Halton 1960).

These randomly generated input patterns (spatiotemporal groundwater abstraction from the production bores and barrier wells) were fed to the numerical simulation model to get the salt concentration (output patterns) at four MLs (B1 = ML1, B3 = ML2, B7 = ML3 and B8 = ML4) by running the calibrated 3D numerical simulation model developed for Tagabe coastal aquifer (Sharan et al. 2024). The salt concentrations after running the numerical model were recorded at the end of 5th year. The model was simulated 130 times with a different set of spatiotemporal pumping patterns to get the salt concentration at four monitoring locations. These pumping patterns and salt concentrations became the input and output patterns, respectively. Using the input–output patterns from the numerical model, several machine learning-based surrogate models were developed in this study.

A limited number of input–output patterns were generated because the intention was to reduce the computational burden in the coupled S-O approach and to determine whether a smaller number of input–output datasets for a large number of variables (70) could be utilised to effectively and accurately train the surrogate models.

2.2. Surrogate and ensemble models

The machine learning-based surrogate and ensemble models were developed to mimic the 3D numerical simulation model of the Tagabe coastal aquifer. The various machine learning and deep learning algorithms could be used to develop surrogate and ensemble models. In this study, numerous machine learning-based models were developed as approximate emulators of the numerical simulation model. This study would be the first to use limited datasets to train numerous machine learning models as surrogate ensembles and decision theories in selecting the best approximators. Past studies have large training datasets and less than five machine learning models as approximate simulators (e.g., Roy and Datta, 2017a; 2017b; Lal and Datta, 2018; 2020). Some of the machine learning and deep learning models used in this study are discussed below.

2.2.1. Artificial neural network

The Artificial Neural Network (ANN) has been widely used in various fields of engineering and science (e.g., Rogers et al. 1995; Shreekanth and Datta 2011; Roy et al. 2024). ANN works similarly to human brains by imitating the process and transferring the information. ANN demonstrates effective performance when tasked with handling complex systems characterised by noisy and ambiguous input data. It can be trained as an approximate simulator of the physical processes (Dhar and Datta 2009). The ANN model is fully connected through neurons in all its layers. ANN has an input layer, one or more hidden layers and an output layer. These layers interact with each other through weighted connections (Yin et al. 2003). The general ANN structure used in this research is shown in Fig. S1.

The mathematical representation of ANN is given in equation (1) (Kumar 2013).

$$y = f_{sigm}\left\{ B_0 \sum_{k=1}^{h}\left[w_k \times f_{sigm}\left(B_{hk} + \sum_{i=1}^{m} w_{ik} x_i \right) \right] \right\} \quad (1)$$

where B_0 = bias at the output layer; w_k = connection weight between the *kth* of the hidden layer and single output neuron; B_{kh} = bias at the *kth* neuron of hidden layer; h = number of neurons in the hidden layer; w_{ik}

= connection weight between the *ith* input element and the hidden layer; x_i = input variable *i*; *y* = output variable; f_{isgm} = transfer function.

2.2.2. Support vector regression

Support Vector Regression (SVR) is an influential machine-learning technique which is not sensitive to local optimum and has minimum over-fitting (Tenne and Goh, 2010). Different kernel functions such as polynomial, Gaussian and linear are used in SVR method. SVR consists of a training dataset: $T = [(a_1, b_1), (a_2, b_2),\ldots,(a_n, b_n)]$ so that a_i is a vector of real independent variables and b_i is the matching scaler real dependent variable. The SV regression equation is given in equation (2) (Parveen et al. 2016).

$$z(a, w) = (w \bullet \delta[a] + k) \tag{2}$$

where *w* = weight vector; *k* is a constant; $\delta[a]$ = feature function; $w \bullet \delta[a]$ = dot product; SVR functions by reducing the equations (3) and (4)

$$Q(f) = C\frac{1}{N}L_{\propto}(b, z[a, w]) + \frac{1}{2}\|w^2\| \tag{3}$$

$$L_{\propto}[b, z(a, w)] = \begin{cases} 0, if|b - z(a, w)| \le \propto \\ |b - z(a, w)| - \propto, otherwise \end{cases} \tag{4}$$

Equation (3) (first term) describes the empirical error (*ee*) where *C* = cost function which is a measure of optimisation among the *ee* and the complexity of the model (second term in equation (3). The cost function controls the SVR problems. Equation (4) illustrates the loss function. The Langrangian multipliers $\gamma_i$andγ_i° transform an optimisation problem into two problems. Using the input support vector a_i, the SVR equation takes the form given in equation (5).

$$z\left(a, \gamma_i - \gamma_i^{\circ}\right) = \sum_{i=1}^{N_{sv}}(\gamma_i - \gamma_i^{\circ})(\delta(a_i) \bullet (\delta(a_j)) + k \tag{5}$$

Further using the support from the kernel function $K(x_i, x_j)$, the SVR can be expressed as equation (6)

$$z\left(a, \gamma_i - \gamma_i^{\circ}\right) = \sum_{i=1}^{N_{sv}}(\gamma_i - \gamma_i^{\circ})K(a, a_i) + k \tag{6}$$

The simple SVR structure is given in Fig. S2.

2.2.3. Genetic programming

The Genetic Programming (GP) model was initially designed by Koza (1992) as an evolutionary algorithm to synthesise programs using the theory of natural selection (Dou et al. 2020). GP is an extension of the genetic algorithm (GA), which employs a generative approach to produce offspring with enhanced fitness by employing fundamental genetic mechanisms such as crossover and mutation. Hierarchical tree formats, comprising predetermined functional and terminal nodes, are used to get the model outcomes. The simple GP model structure (tree) is given in Fig. S3. Using the figure, the functional expression can be expressed using equation (7).

$$y(k) = (-y_{k-1}) + (0.2 \times (-u_{k-1})) \tag{7}$$

2.2.4. Multivariate adaptive regression spline

The Multivariate Adaptive Regression Spline (MARS) model was developed by Friedman (1991) and uses a nonparametric adaptive regression adaptive search strategy in which forward and backward stages modify the search space. MARS is capable of predicting continuous and binary output variables, which makes it an accurate and flexible machine learning model (Salford Predictive Modeler 2019). MARS categorises and divides the complete input variables into different intervals and creates the regression model by matching single splines to each interval. The process of building a MARS model involves iteratively adding piecewise linear functions called basis functions to improve the fit of the model. These basis functions, including hinge functions and constant functions, are chosen based on their ability to decrease the residual sum of squares, ensuring a better fit to the data.

MARS starts with a simple model, typically a constant term representing the mean response, and then progressively adds basis functions in a forward pass to increase the model's complexity. Subsequently, a backward pass is performed to remove redundant basis functions and simplify the model, thus preventing overfitting. The resulting MARS model provides a balance between flexibility and interpretability, making it valuable for capturing complex relationships in data while remaining comprehensible to users (Friedman 1991; Salford Predictive Modeler 2019).

MARS can be further divided into two models: Multivariate Adaptive Regression Spline with Piecewise Cubic Spline (MARS-C) and Multivariate Adaptive Regression Spline with Piecewise Linear (MARS-L). MARS-C uses piecewise cubic splines to model relationships, offering greater flexibility at the cost of increased complexity and potential overfitting. MARS-L, on the other hand, employs piecewise linear functions, which are simpler and may be more interpretable, with potentially lower risk of overfitting, particularly in cases with limited data.

The MARS model can be mathematically represented using equation (8).

$$\widehat{y} = c_o + \sum_{m=1}^{M} c_m B_m(x) \tag{8}$$

where $\widehat{y}$ = dependent variable; c_o = constant; $B_m(x)$ = *m*th basin function; c_m = coefficient of the *m*th basin function.

2.2.5. Probabilistic linear regression

Probabilistic linear regression (PLR) enhances traditional linear regression by incorporating uncertainty into both model parameters and predictions (Bishop 2006). Instead of offering singular point estimates for the response variable based on predictor variables, probabilistic linear regression estimates a probability distribution over potential response variable values, which accounts for inherent noise in the data and uncertainty in model parameters (Gelman et al. 2013). Typically, it assumes a Gaussian distribution for the response variable, with the mean predicted by the linear combination of predictor variables and the variance representing prediction uncertainty (Bishop 2006).

Bayesian methods, such as Bayesian linear regression, are often employed to infer the posterior distribution of model parameters, leveraging prior knowledge or beliefs about parameters and updating them based on observed data (Gelman et al. 2013). This results in a posterior distribution that comprehensively represents uncertainty in both model parameters and predictions (Bishop 2006), providing numerous advantages, including robustness to outliers, incorporation of prior knowledge, and the ability to quantify uncertainty, making it a powerful tool in various applications such as decision-making, forecasting, and risk assessment (Gelman et al. 2013).

The mathematical representation of PLR, incorporating uncertainty into both model parameters and predictions is given in equation (9) and the simple graphical representation of PLR is shown in Fig. S4.

$$Y = \beta_0 + \beta_1 x + \varepsilon \tag{9}$$

where ε = random error; x = independent variable; y = dependent variable; β_0 = population Y intercept; β_1 = population slope coefficient.

2.2.6. Random forest regression

Random Forest Regression (RFR) is an ensemble learning technique that combines the predictions of multiple decision trees to improve predictive accuracy and robustness. In Random Forest regression, a collection of decision trees is trained on randomly selected subsets of the data and predictor variables. During training, each tree learns to predict the response variable based on a subset of the features and a random subset of the training data. When making predictions, each tree in the forest produces an individual prediction, and the final prediction is

obtained by averaging or taking a weighted average of the predictions from all the trees. This ensemble approach helps to mitigate overfitting and provides more stable and accurate predictions compared to individual decision trees. Additionally, Random Forest regression can handle both numerical and categorical data, as well as missing values, making it a versatile and powerful regression technique (Breiman 2001).

The random forest does not have a single regression equation like traditional linear regression. Fig. S5 shows the RFR using decision trees.

2.2.7. Group method of data handling

The Group Method of Data Handling (GMDH) is a computational algorithm used for modelling complex relationships in data by iteratively selecting and combining simpler mathematical models. GMDH works by progressively refining the model structure through a process of self-organisation and optimisation. Initially, the algorithm generates a pool of potential models, often simple polynomial or linear models. These models are evaluated based on some criterion, such as their predictive accuracy or goodness of fit. Subsequently, GMDH selects the best-performing models and combines them to create more complex models. This process continues iteratively, with the algorithm refining the model structure at each step by selecting and combining models that lead to improved performance. GMDH is known for its ability to automatically generate and optimise models without prior assumptions about the underlying data distribution, making it useful for a wide range of applications in data analysis and modelling (Ivakhnenko 1968).

2.2.8. Long Short-Term Memory

Long Short-Term Memory (LSTM) is a type of recurrent neural network (RNN) architecture designed to address the vanishing gradient problem in traditional RNNs, enabling them to effectively model and learn long-term dependencies in sequential data. LSTM networks consist of memory cells that maintain a state over time and three gates: input gate, forget gate, and output gate. These gates regulate the flow of information into and out of the memory cells, allowing LSTMs to selectively remember or forget information at each time step. This mechanism enables LSTMs to capture temporal dependencies and patterns in sequential data, making them particularly well-suited for tasks such as time series prediction, natural language processing, and speech recognition. By retaining important information over long sequences and mitigating the effects of the vanishing gradient problem, LSTM networks can learn and represent complex temporal dynamics in data with greater effectiveness (Hochreiter and Schmidhuber 1997).

Bidirectional Long Short-Term Memory (Bi-LSTM) is an extension of the traditional LSTM (Long Short-Term Memory) recurrent neural network architecture. Bi-LSTM networks enhance the capabilities of LSTM networks by processing input sequences in both forward and backward directions simultaneously.

2.2.9. Adaptive Neuro-Fuzzy Inference Systems

Adaptive Neuro-Fuzzy Inference Systems (ANFIS) combine the adaptability of neural networks with the interpretability of fuzzy logic systems to create hybrid models capable of handling complex nonlinear relationships in data (Jang 1993). ANFIS models consist of a series of fuzzy if-then rules that are optimised using a hybrid learning algorithm, typically a combination of gradient descent and least squares methods. These rules are organised in a hierarchical structure, with each rule representing a local model capturing a specific region of the input space. The parameters of the fuzzy membership functions and the linear coefficients associated with each rule are adjusted during training to minimise the error between the model's output and the actual data.

The ANFIS learning algorithm proceeds in two phases: a forward pass and a backward pass. During the forward pass, the input data is propagated through the fuzzy inference system to compute the output of each rule. These outputs are then combined to produce the overall model output. In the backward pass, the gradient of the error with respect to the model parameters is computed, and the parameters are updated using gradient descent to minimise the error. ANFIS models offer several advantages, including their ability to capture complex nonlinear relationships, their interpretability due to the fuzzy rule base, and their flexibility in handling both numerical and categorical data. However, they also have limitations, such as the need for careful selection of fuzzy rules and membership functions and the potential for overfitting if not adequately regularised.

2.2.10. Asynchronous successive halving algorithm tuned automatic model selection

The Asynchronous Successive Halving Algorithm tuned Automatic Model Selection (AMS-AHSA) methodology integrates the Asynchronous Successive Halving Algorithm with Automatic Model Selection to automate the process of identifying the optimal machine learning model and its associated hyperparameters for a given dataset. This approach begins by defining a set of candidate models, each with its hyperparameters. Subsequently, the Asynchronous Successive Halving Algorithm is employed, which systematically prunes underperforming models and allocates more resources to promising ones in an asynchronous manner. This process continues through successive rounds until a subset of the best-performing models remains. Finally, based on the performance estimates obtained during the algorithm's execution, the best-performing model and its hyperparameters are selected. AMS-AHSA efficiently navigates the model space to facilitate automated model selection, which is particularly beneficial in resource-constrained or large-scale hyperparameter optimisation scenarios (Yang et al. 2019).

2.2.11. Bayesian optimisation tuned automatic model selection

Bayesian Optimisation tuned Automatic Model Selection (AMS-B) is a sophisticated approach that integrates the power of Bayesian Optimisation (BO) with Automatic Model Selection (AMS) to automate the selection of the most suitable machine learning model and its associated hyperparameters for a given dataset. AMS-B harnesses Bayesian Optimization's efficiency in exploring the model space to automate the model selection process and identify high-performing models with minimal manual intervention. This methodology is particularly valuable in scenarios where manual model selection and hyperparameter tuning are time-consuming and resource-intensive (Snoek et al. 2012).

2.3. Management model

The ensemble models developed were externally linked to the CEMOGA (Deb and Goel 2001) optimisation algorithm to obtain optimal groundwater extraction values for developing a management model. The multi-objective saltwater water intrusion management model was developed to find robust SWI management strategies for the Tagabe coastal aquifer. The steps involved in developing the management model are summarised in the flow diagram shown in Fig. 2.

The management model developed in the current study has a multi-objective type problem of two conflicting objectives. The objectives of the management model include maximising the freshwater abstraction from pumping/production wells (PWs) for beneficial purposes and minimising the pumping from barrier wells (BWs). BW pumping is reduced because it would be an issue to dispose of the saline water if it is abstracted in high volumes. According to Datta and Peralta (1986), the management model solutions would provide Pareto optimal front. The Pareto optimal front would provide the water managers and policy-makers with the trade-off between two conflicting solutions. The management model can be mathematically represented in equations (10) to (15) (Bhattacharjya and Datta 2005).

$$\text{Maximise}: f_1(Q_{PW}) = \sum_{n=1}^{N}\sum_{t=1}^{T} Q^t_{PW_n} \tag{10}$$

$$\text{Minimise}: f_2(Q_{BW}) = \sum_{m=1}^{M}\sum_{t=1}^{T} Q^t_{BW_m} \tag{11}$$

Subject to

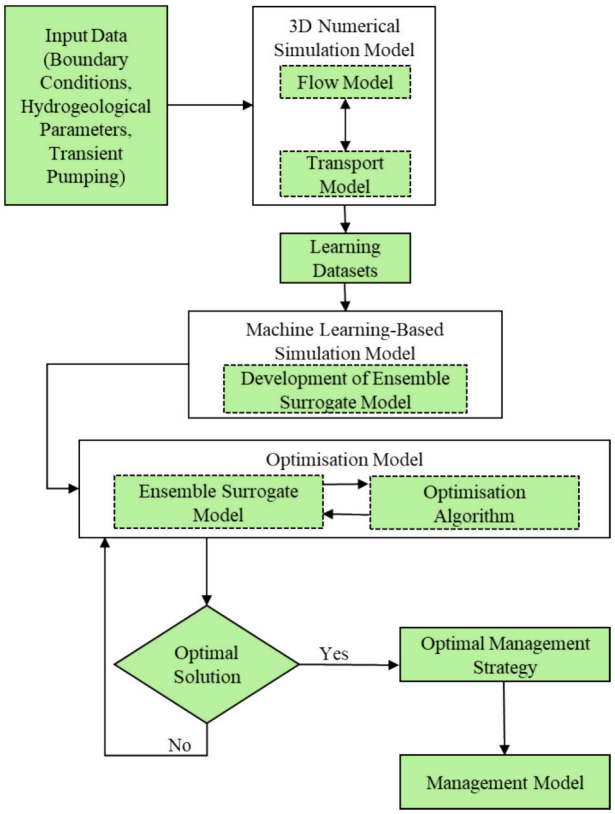


Fig. 2. Flow diagram of linked simulation-optimisation management model.

$$C_i = \varepsilon(Q_{PW}, Q_{BW}) \tag{12}$$

$$C_i \le C_{max} \forall_i \tag{13}$$

$$Q_{PW_{min}} \le Q^t_{PW_n} \le Q_{PW_{max}} \tag{14}$$

$$Q_{BW_{min}} \le Q^t_{BW_n} \le Q_{BW_{max}} \tag{15}$$

where PW = pumping/production well, BW = barrier well; where$Q^t_{PW_n}$ = water extraction from the nth production well during tth time steps; $Q^t_{BW_m}$ = water extraction from the nth barrier well during tth time steps; C_i = saltwater concentrations at the ith MLs at the end of the management period; $\varepsilon()$ denotes the density-dependent coupled flow and salt transport surrogate model. The constraint given in equation (12) shows the linking of the surrogate ensemble model with the optimisation model; the constraint given in equation (13) indicates the maximum allowable salt concentration at various MLs; the constraints given in equations (14) and (15) outline the upper and lower limits of the water abstraction from pumping and barrier wells, respectively.

2.4. Model performance evaluation criterion

Various performance evaluation criteria were used to assess the performances of the surrogate models. Correlation coefficient or Pearson's correlation coefficient (R^2) (PCC), Index of Agreement (IoA), Kling-Gupta efficiency (KGE), Nash-Sutcliffe efficiency coefficient (NSE), mean absolute error (MAE), root mean square error (RMSE) and mean absolute percentage error (MAPE) were used to evaluate the performance of surrogate and ensemble models.

2.5. Shannon's entropy-based decision theory

Twelve surrogate models were developed for each ML, along with ensembles of the selected surrogate models for each of the four MLs. Shannon's entropy weight-based decision theory (Shannon 1948) was applied to select the best-performing model. Entropy weight-based decision theory in model selection employs the concept of entropy to assign weights to different models based on their performance and uncertainty. Shannon's entropy weights (EW) consist of five steps in ranking the models (Li et al. 2011). The steps are as follows:

a). Calculating the entropy value for each index using Shannon's Entropy principles. The entropy value for the jth index was determined using the equations (16) – (18).

$$Entropy_j = -k\sum_{i=1}^{m} f_{ij} \ln f_{ij} \tag{16}$$

$$f_{ij} = S_{ij} \div \sum_{i=1}^{m} S_{ij} \tag{17}$$

$$k = 1 \div \ln m \tag{18}$$

b). Determining the entropy weight for each index. The entropy weight for the jth index was calculated using equation (19).

$$w(entropy)_j = \frac{1 - entropy_j}{P - \sum_{j=1}^{P} entropy_j} \tag{19}$$

EW (equation (19) signifies the index's importance in decision-making. A higher value of EW suggests that the index contains more information and is more critical in the decision-making process.

c). Determining the rank weight for each model involves adding up the result of multiplying each index's EW by the standardised value of that index. This process is expressed mathematically in equation (20).

$$w(entropy)_i = \sum_{j=1}^{P} S_{ij} \times w(entropy)_j \tag{20}$$

d). Equation (21) gives the step in determining the model ranking.

$$\max[w(entropy)_i], \cdots, \min[w(entropy)_i]; \text{for} i = 1, 2, \cdots, m \tag{21}$$

e). Finally, the EWs for individual surrogate prediction models are calculated using equation (22).

$$w(entropy)_i = w(entropy)_i \div \sum_{i=1}^{m} w(entropy)_i \tag{22}$$

This approach considers the accuracy of each model and the diversity and reliability of their predictions. By incorporating EW, decision-makers can account for the complexity and uncertainty inherent in real-world datasets, thus making more informed choices when selecting the most suitable model (Wang et al. 2007). This methodology offers a principled way to balance the trade-offs between model accuracy and robustness, ensuring that the selected model effectively captures the underlying patterns in the data while accounting for uncertainty and variability.

3. Results and discussion

3.1. Numerical simulation model

The SEAWAT-based numerical simulation model was developed for Tagabe coastal aquifer in Vanuatu. The model indicated that with the current pumping regimes, the SWI rates would increase in Tagabe coastal aquifer. Four scenarios were simulated using the calibrated and validated numerical model to investigate and find the best SWI management strategies. These scenarios included increased population and freshwater pumping rates, the addition of barrier wells and injection wells to prevent saltwater encroachment into freshwater wells, and the effect of rising sea levels on the SWI rates in Tagabe coastal aquifer. The results from the four scenarios are shown in Fig. 3.

The Tagabe coastal aquifer, which supplies water to the capital city

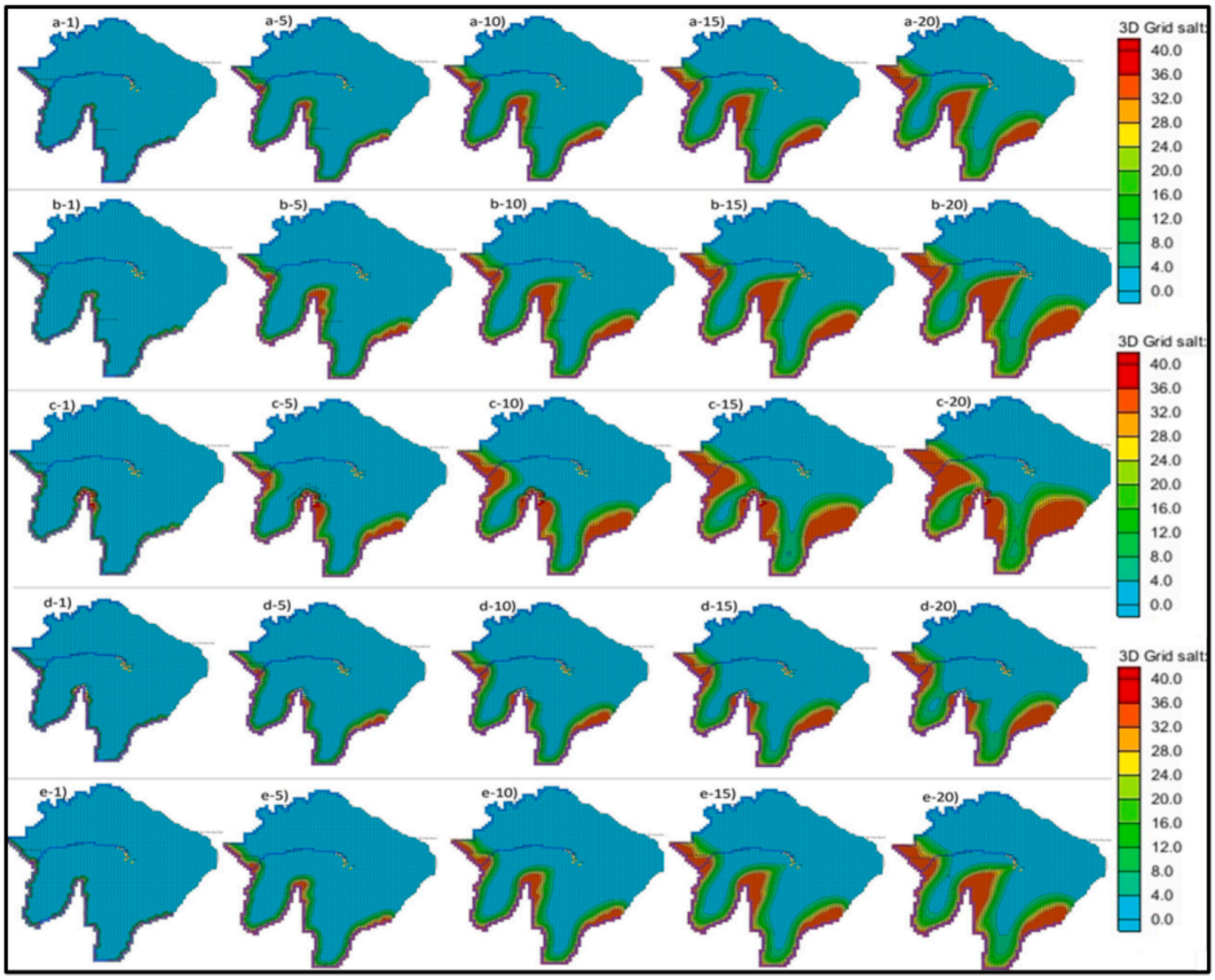


Fig. 3. (a-1 to a-20) shows the plan view of the simulated results of saltwater intrusion for the base case; (b-1 to b-20) increasing the pumping and number of pumping wells (scenario 1); (c-1 to c-20) addition of barrier wells (scenario 2); (d-1 to d-20) addition of injection well plus barrier wells (scenario 3); (e-1 to e-20) sea level rise (scenario 4). The numbers 1, 5, 10, 15 and 20 represent the time steps 1 year, 5 years, 10 years, 15 years and 20 years, respectively. .
Source (Sharan et al. 2024)

of Vanuatu, has eight operational boreholes. Using current field pumping data, the MODFLOW model interpolated transient pumping data over a 20-year period to predict SWI in the aquifer. The calibrated model ran for 20 years, recording the SWI. Fig. 3 (a-1 to a-20) shows the plan view of the model domain for the base case, with results recorded at five different time steps. The numbers 1, 5, 10, 15, and 20 correspond to 1-year, 5-year, 10-year, 15-year, and 20-year time steps, respectively. The contours represent the SWI in the Tagabe coastal aquifer, with red indicating salt concentrations greater than 30 kg/m^3 and light blue indicating approximately 0 kg/m^3.

The addition of barrier wells and injection wells has significantly reduced the SWI rates as shown in Fig. 3 (d-1 to d-20). Sea level rise (SLR) (Fig. 3. e-1 to e-20) has some positive effect on the rates of SWI in Tagabe coastal aquifer. In the current simulation, the SLR was only increased by 25 cm upto 20 years (2043). If the sea level rises by over 1 m, then the effects would be immense. Sharan et al. (2023; 2024) reported a similar SLR effect in coastal aquifers.

In addition, the results also indicated that the increased freshwater pumping from the production bores in Tagabe coastal aquifer would cause higher rates of SWI. To manage SWI, barrier well and injection well pumping would be required to reverse the hydraulic gradient and prevent the saline water from entering the production bores. Moreover, sea level rise affects SWI rates in Tagabe coastal aquifer. Similar results were reported by Sharan et al. (2024).

The numerical model predicted that increasing the pumping rates with the increased population in future would contaminate the freshwater bores in Tagabe coastal aquifer with increased salinity. Moreover, the model also predicted that using hydraulic barriers would decrease the SWI. However, the use of barrier wells and injection wells is costly. Also, the disposal of abstracted saline water from the barrier wells or the freshwater supply needed to inject into the aquifer to reverse the hydraulic gradients could be an issue. Therefore, optimal SWI management strategies must be provided where the minimum barrier well pumping is required, and maximum allowable salt concentration is allowed in the production bores with the maximum pumping rates. Due to conflicting criteria, this problem can only be tackled with linked simulation-optimisation techniques.

3.2. *Surrogate and ensemble model*

The input and output patterns gathered from the 3D numerical simulation model were used to develop twelve surrogate and four

ensemble models at different (four) MLs. In addition, the twelve surrogate models were ranked using Shannon's entropy and the top five surrogate models (at each of the MLs) were used to develop the weighted average ensembles. The number of input–output patterns was limited based on the computational time taken (20 min) by the numerical model. Additionally, the output (salt concentrations) showed minimal variation across all machine learning-based models. Hence, a total of 130 input–output patterns were used to train and test the surrogate models. 80% of the dataset was used to train the surrogates and 20% to test the surrogate models against the actual salt concentrations. MATLAB was used to train the twelve surrogate models and the linear regression graphs were used to compare the actual and predicted values of salt concentrations generated by different algorithms. The actual versus predicted during the training stage is given in Figs. S6 – S9. A limited number of datasets were chosen to achieve computational efficiency from running the numerical model. One of the novelties of the current study was the use of a limited number of input–output patterns. The results indicated that despite using limited training datasets, the surrogates were trained and predicted salt concentrations reasonably well.

Fig. S6. (a-l) shows the actual versus predicted regression analysis of twelve different machine learning models for ML1 during the training period. The majority of the machine learning models predicted better salt concentrations for ML1. The models ANFIS, ANN, MARS_L and GPR outperformed with the R^2 greater than 0.96. Bi-LSTM gave poor prediction results at ML1. Fig. S7. (a-l) shows the actual versus predicted regression analysis of twelve different machine learning models for ML2 during the training period. The models ANFIS, MARS_L, AMS_ASHA and GPR outperformed at ML2 with the R^2 greater than 0.98. PLR and SVR also performed well with R^2 greater than 0.92. For ML2, ANN, Bi-LSTM and RF did not perform well. Similarly, Fig. S8. (a-l) shows the actual versus predicted regression analysis of twelve different machine learning models for ML3 during the training period. For ML3, ANFIS, MARS_L, AMS_Bayesian, GPR and RF performed exceptionally well during the training period compared with other machine learning models. Prediction of salt concentration at ML4 [Fig. S9. (a-l)] was exceptionally predicted by MARS_C, MARS_L, AMS_ASHA, and RF. ANN, Bi-LSTM, and SVR did not perform well in predicting accurate results.

After training the twelve models using the 80% dataset, the 20% dataset was used to test the performance of the models. The results of actual versus predicted salt concentrations during the testing periods are given in Figs. S10 – S13. Fig. S10 (a-l) shows the actual versus predicted salt concentrations of twelve surrogate models at ML1. ANFIS, ANN, AMS_Bayesian, AMS_ASHA, GPR, PLR and SVR showed similar patterns of salt concentrations to the actual ones. Similarly, at ML2, MARS_C, MARS_L, AMS_ASHA, GPR, PLR and SVR displayed very close patterns of salt concentrations when compared with the actual values, as shown in Fig. S11 a, c, d, f, i, j and l, respectively.

The ML3 predicted values of salt concentrations by the surrogates are not up to the levels as compared to ML1 and ML2 because the salt concentrations (output patterns) at ML3 were quite similar, which resulted in poor-performing surrogates. However, MARS_C, MARS_L, GPR and RF displayed patterns similar to the actual values, as shown in Fig. S12 c, d, i and k, respectively. The predicted salt concentrations at ML4 during the testing stage are given in Fig. S13 (a-l). The output displayed the variations and patterns following the actual values of salt concentrations. However, only a few surrogates were able to estimate the outputs close to the inputs. These surrogates were MARS_C, MARS_L and RF. Other surrogates did not show many variations in their outputs and followed the patterns of the actual values.

3.3. Model performance and selection

The different criteria for measuring the performance of the surrogate models for different ML during the model training given in Table 2 and Fig. 4. These performances are for the training stage, where the actual

Table 2
Performance criteria of twelve surrogate models at four different monitoring locations (MLs) during the model training period.

	Performance Measure	ANFIS	ANN	MARS_C	MARS_L	AMS_Bayesian	AMS_ASHA	BiLSTM	GMDH	GPR	PLR	RF	SVR
ML1	Mean Absolute Deviation (MAD)	0.0009293	0.0017723	0.0017369	0.0000927	0.0048193	0.0020226	0.0052974	0.0038625	0.0005386	0.0021990	0.0025491	0.0028542
	Mean Square Error (MSE)	0.0000017	0.0000045	0.0000052	0.0000000	0.0000373	0.0000067	0.0000495	0.0000223	0.0000005	0.0000078	0.0000117	0.0000118
	RMSE	0.0012968	0.0021187	0.0022825	0.0001138	0.0061111	0.0025953	0.0070324	0.0047200	0.0006848	0.0027999	0.0034223	0.0034335
	MAPE (%)	0.303	0.580	0.568	0.030	1.570	0.663	1.754	1.263	0.176	0.720	0.837	0.932
ML2	Mean Absolute Deviation (MAD)	0.001235	0.010136	0.003231	0.000171	0.009189	0.000074	0.010648	0.005414	0.000100	0.002983	0.008319	0.001147
	Mean Square Error (MSE)	0.000003	0.000168	0.000017	0.000000	0.000141	0.000000	0.000214	0.000050	0.000000	0.000015	0.000117	0.000011
	RMSE	0.001600	0.012966	0.004155	0.000212	0.011885	0.000101	0.014639	0.007071	0.000128	0.003913	0.010814	0.003376
	MAPE (%)	0.459	3.840	1.197	0.063	3.371	0.027	4.102	2.020	0.037	1.114	3.142	0.433
ML3	Mean Absolute Deviation (MAD)	0.0009339	0.0020962	0.0012951	0.0000495	0.0005557	0.0008921	0.0023394	0.0013296	0.0001112	0.0020018	0.0001535	0.0020977
	Mean Square Error (MSE)	0.0000017	0.0000198	0.0000028	0.0000000	0.0000005	0.0000121	0.0000230	0.0000150	0.0000001	0.0000173	0.0000003	0.0000198
	RMSE	0.0012984	0.0044534	0.0016758	0.0000625	0.0007043	0.0034716	0.0047910	0.0038725	0.0002292	0.0041651	0.0005843	0.0044534
	MAPE (%)	0.309	0.714	0.433	0.016	0.185	0.313	0.791	0.459	0.038	0.681	0.054	0.714
ML4	Mean Absolute Deviation (MAD)	0.0008730	0.0018996	0.0004841	0.0000299	0.0016707	0.0003444	0.0026600	0.0006084	0.0006741	0.0018773	0.0001878	0.0019016
	Mean Square Error (MSE)	0.0000013	0.0000045	0.0000004	0.0000000	0.0000053	0.0000002	0.0000117	0.0000007	0.0000007	0.0000043	0.0000000	0.0000045
	RMSE	0.0011613	0.0021146	0.0006191	0.0000366	0.0023100	0.0004946	0.0034221	0.0008436	0.0008286	0.0020803	0.0001883	0.0021146
	MAPE (%)	0.292	0.636	0.162	0.010	0.557	0.115	0.893	0.204	0.226	0.628	0.063	0.636

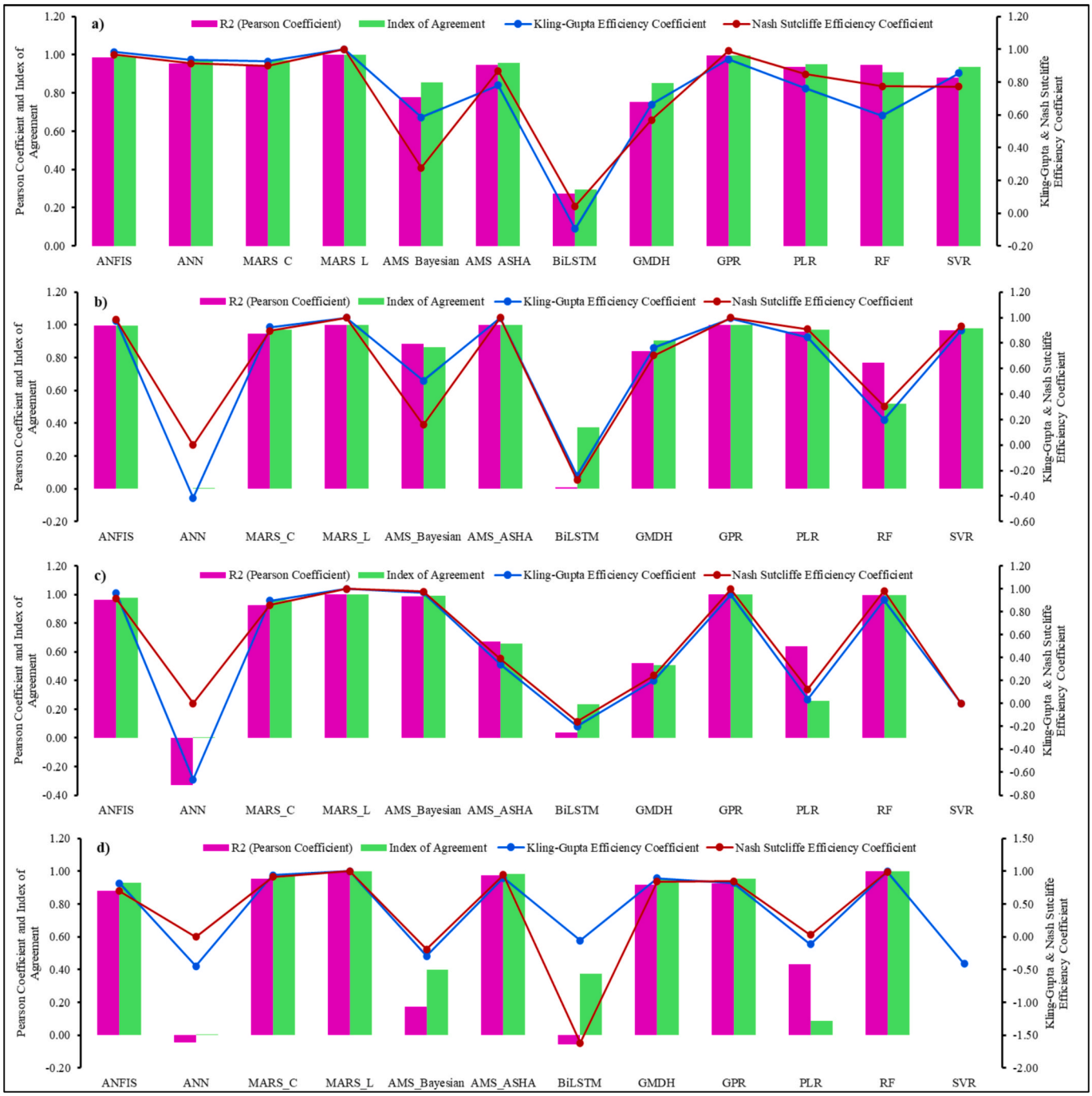


Fig. 4. Performance of all surrogate models during the training stage using Pearson correlation coefficient, Index of Agreement, Kling-Gupta Efficiency coefficient and Nash-Sutcliffe Efficiency coefficient at **a)** ML2, **b)** ML2, **c)** ML3 and **d)** ML4.

values of the salt concentration were compared with the predicted values by various machine learning models mentioned in section 2.2. The majority of the models performed better in predicting the salt concentration during the testing period. Comparing the MAPE (%), Pearson's coefficient, Index of Agreement, Kling-Gupta efficiency and Nash Sutcliffe efficiency coefficients, it can be seen that ANFIS, ANN, MARS_C, MARS_L, AMS_ASHA, GPR and SVR predicted better salt concentrations. Similarly, ANFIS, MARS_C, MARS_L, AMS_ASHA, GPR, PLR and SVR performed better in predicting the salt concentrations at ML2 during the training stage. ANFIS, MARS_C, MARS_L, AMS_Bayesian, GPR and RF performed better in predicting the salt concentrations at ML3 during the training stage. Finally, MARS_C, MARS_L, AMS_ASHA, GMDH and RF performed better in predicting the salt concentrations at ML4 during the training stage.

Table 3 and Fig. 5 demonstrate the reliable performance of twelve surrogate models at different MLs during the testing period. The actual and predicted salt concentrations were compared using the MAPE (%), Pearson's coefficient, Index of Agreement, Kling-Gupta efficiency, and Nash-Sutcliffe efficiency coefficients. ANN, AMS_Bayesian and PLR consistently predicted better salt concentrations at ML1. ANFIS, MARS_C, MARS_L, AMS_Bayesian, AMS_ASHA, GHD and SVR consistently predicted better salt concentrations at ML2. In addition, the reliable surrogate models in predicting the salt concentrations at ML3 were AMS_Bayesian and ANN. Meanwhile, ANFIS, AMS_ASHA, and SVR performed well. All ensemble models consistently performed better, as shown in Table 3.

Table 3
Performance criteria of twelve surrogate models and four ensemble models at four different monitoring locations (MLs) during the model testing period.

	Performance Measure	ANFIS	ANN	MARS_C	MARS_L	AMS_Bayesian	AMS_ASHA	BiLSTM	GMDH	GPR	PLR	RF	SVR	Ensemble
ML1	Mean Absolute Deviation (MAD)	0.008200	0.006349	0.007465	0.008784	0.006097	0.005403	0.006612	0.006838	0.005481	0.005194	0.006468	0.005891	0.005640
	Mean Square Error (MSE)	0.000106	0.000072	0.000111	0.000149	0.000060	0.000068	0.000121	0.000112	0.000066	0.000062	0.000106	0.000074	0.000064
	RMSE	0.010318	0.008478	0.010540	0.012212	0.007752	0.008220	0.011006	0.010560	0.008094	0.007874	0.010290	0.008610	0.007997
	MAPE (%)	2.718	2.072	2.528	2.965	2.045	1.839	2.270	2.333	1.861	1.767	2.210	1.998	1.909
ML2	Mean Absolute Deviation (MAD)	0.01127	0.01195	0.00480	0.00693	0.01124	0.00513	0.01089	0.00620	0.00629	0.00611	0.01070	0.00590	0.00383
	Mean Square Error (MSE)	0.00016	0.00020	0.00003	0.00007	0.00019	0.00005	0.00026	0.00006	0.00007	0.00006	0.00016	0.00006	0.00003
	RMSE	0.01282	0.01408	0.00570	0.00819	0.01364	0.00682	0.01603	0.00770	0.00815	0.00783	0.01251	0.00767	0.00548
	MAPE (%)	4.169	4.465	1.808	2.569	4.232	1.945	4.245	2.345	2.396	2.330	4.036	2.237	1.469
ML3	Mean Absolute Deviation (MAD)	0.006016	0.001744	0.004818	0.005643	0.003692	0.003950	0.002270	0.005475	0.002075	0.001717	0.003989	0.001750	0.001563
	Mean Square Error (MSE)	0.000052	0.000021	0.000053	0.000055	0.000034	0.000035	0.000025	0.000071	0.000024	0.000022	0.000038	0.000021	0.000021
	RMSE	0.007226	0.004616	0.007253	0.007393	0.005832	0.005922	0.005031	0.008440	0.004896	0.004698	0.006124	0.004620	0.004545
	MAPE (%)	2.019	0.585	1.632	1.904	1.254	1.341	0.777	1.849	0.716	0.596	1.354	0.606	0.544
ML4	Mean Absolute Deviation (MAD)	0.0032556	0.0013282	0.0040002	0.0040240	0.0005095	0.0039669	0.0038250	0.0027744	0.0031787	0.0013349	0.0040280	0.0013341	0.0010268
	Mean Square Error (MSE)	0.0000180	0.0000020	0.0000171	0.0000180	0.0000004	0.0000160	0.0000231	0.0000096	0.0000147	0.0000020	0.0000166	0.0000020	0.0000012
	RMSE	0.0042461	0.0014021	0.0041331	0.0042417	0.0006236	0.0039962	0.0048019	0.0030969	0.0038287	0.0014056	0.0040709	0.0014080	0.0011007
	MAPE (%)	1.096	0.445	1.348	1.356	0.172	1.336	1.289	0.935	1.071	0.450	1.357	0.450	0.346

An absolute error boxplot was also used to compare standalone surrogate models, as shown in Fig. 6. The boxplots revealed that different surrogates perform differently for all four MLs. Also, most surrogate models performed better according to the multiple criteria mentioned in Section 2.4. However, different prediction models may excel in various performance metrics. For example, one model might show superior performance in correlation coefficient, while another might perform better in relative error. To reconcile these differences, a comprehensive set of performance metrics should be employed in the decision-making process to address such contradictions objectively. This method categorises performance metrics into benefit indices (where higher values are preferred) and cost indices (where lower values are preferred) (Roy et al. 2021). This study utilised four benefit and four cost indices to evaluate prediction model accuracy. Decision-making involved calculating the weights of each hybridised model using these indices, aided by Shannon's Entropy concepts.

The Shannon's entropy weight (EW) was used to select the best-performing surrogate model based on their weights. The EWs of the performance indices are given in Table 4. The higher the entropy weight value of the performance indices, the greater its impact on determining the weight of the individual models. That is to say, higher values of the EW of the performance indices indicate the greater impact of this index in the decision-making process. The EWs of individual prediction models were calculated to rank the best-performing surrogate model in predicting the salt concentrations at four MLs. The ranking of the surrogate model was solely based on their EWs. The surrogate model ranking based on EWs is shown in Table 5.

EWs easily allowed the ranking of best-predicting models. The ranking of surrogate models was used to develop an ensemble model that would predict better results than the standalone surrogate models. The top-ranked five surrogate models were used to form the ensembles at each of the MLs. Although combining a larger number of surrogates to form an ensemble provides better assurance in predicting salt concentrations, it may also incur a computational burden, particularly in the development of a coupled S-O-based saltwater intrusion management model. As such, the number of surrogate models in the ensemble formation was limited to the top five, as determined by Shannon's entropy. Hence, five surrogates were chosen to form an ensemble model for predicting the salt concentrations at ML1. Based on the EW ranking given in Table 5, the ensemble model for ML1 was formulated using ANN, AMS_Bayesian, PLR, GPR and AMS_ASHA.

Similarly, the ensemble at ML2 included MARS_C, AMS_ASHA, SVR, PLR and MARS_L. The ensemble model consisted of ANN, SVR, PLR, GPR and BiLSTM surrogate approximators for ML3. Lastly, the surrogates used to develop an ensemble model at ML4 were AMS_Bayesian, ANN, PLR and SVR. For ML4, only four surrogates were used in forming the ensemble model because using the fifth surrogate (GPR) based on ranking gave poor results. The performance of four ensemble models is given in Table 3. The results indicated that all the ensemble models performed better than the standalone surrogate models. The residual of the ensemble surrogate model is also shown in Fig. 7. The residuals indicate fewer variations between the actual and predicted salt concentrations at different MLs.

3.4. Management model

The four ensemble models developed at the MLs were separately linked with the CEMOGA, and a multi-objective saltwater intrusion management model was formulated for the Tagabe coastal aquifer. The two conflicting objectives of the management model were maximising the production well pumping and minimising the barrier well pumping. The constraint of the optimisation formulation was to maintain a specific maximum permissible salt concentration at different MLs. Several combinations of different parameters were simulated using different optimum parameter values in optimisation formulation.

The population size is an important factor that determines how many

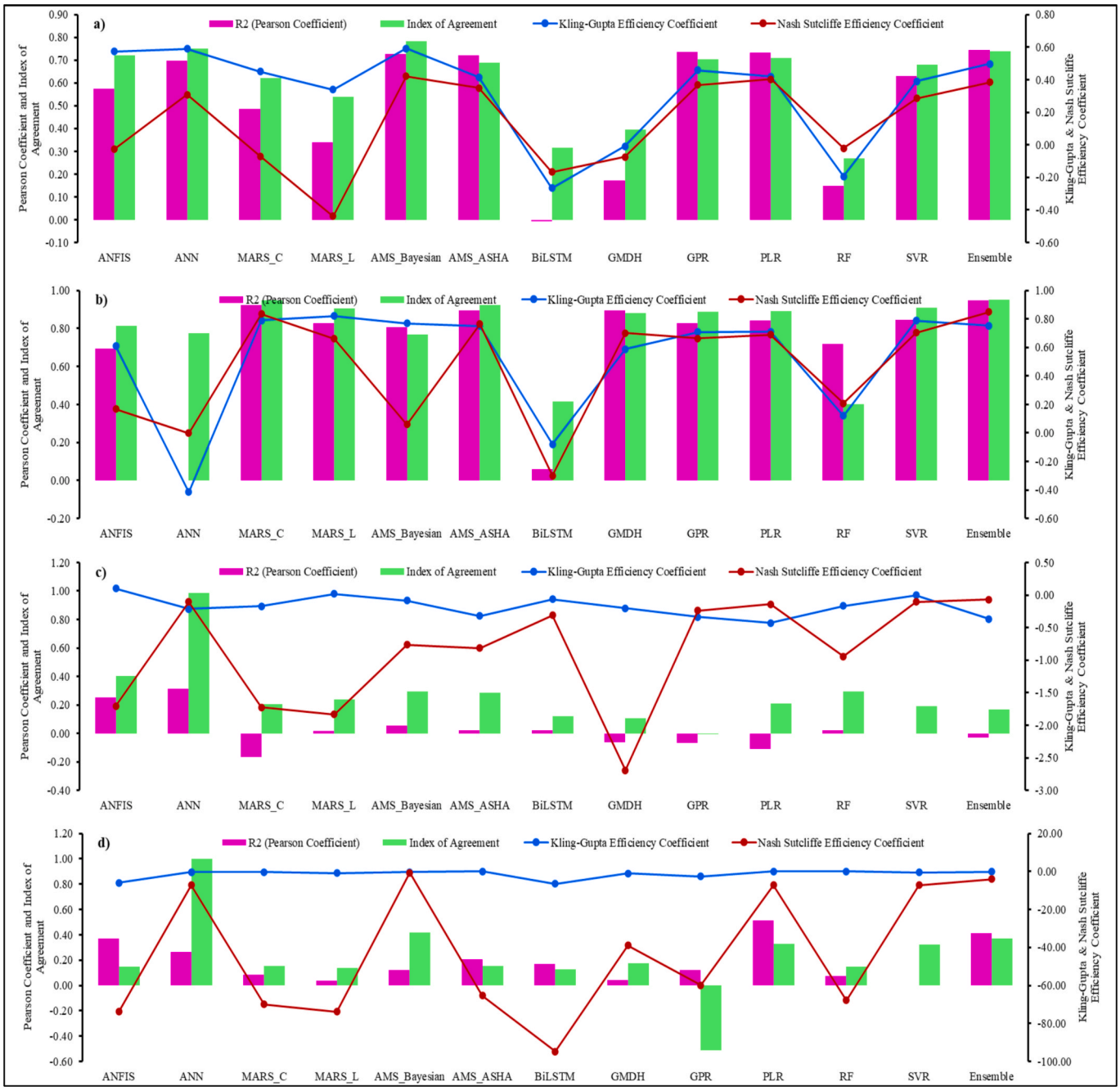


Fig. 5. Performance of all surrogate models during the training stage using Pearson correlation coefficient, Index of Agreement, Kling-Gupta Efficiency coefficient and Nash-Sutcliffe Efficiency coefficient at **a)** ML2, **b)** ML2, **c)** ML3 and **d)** ML4.

individuals are present in each generation of a genetic algorithm. Having a large population size enables the algorithm to explore the solution space more extensively, improving the likelihood of finding a global solution. Conversely, a smaller population size limits the search space and impacts the distribution of solutions along the Pareto optimal front. This study selected a population size of 2,000 to balance population diversity and computational efficiency based on various trials and the interplay with other parameters.

The optimisation algorithm was executed for 16,000 generations to achieve the global optimal solution. This required a total of 32,000,000 evaluations, calculated as 2,000 individuals per generation multiplied by 16,000 generations. The algorithm employed a tournament selection method with a tournament size of two. The crossover and mutation rates were set at 0.92 and 0.1, respectively. The migration parameter used a forward direction with a fraction of 0.2 and an interval of 20. A Pareto front population fraction of 0.7 was used, resulting in 1,400 (2,000 × 0.7) non-dominated optimal solutions from the 2,000 individuals. The function and constraint tolerances were set at 1×10^{-4}. The optimisation routine took 11,354 s to converge to optimal solutions.

The Pareto-optimal front obtained by CEMOGA-ensemble models are shown in Fig. 8.

The 1400 Pareto optimal front solutions related to groundwater abstractions from the combined eight production bores and six barrier wells are shown in Fig. 8. This Pareto optimal front provides numerous solutions for maximising pumping from the production wells and minimising the pumping from the barrier wells while maintaining the allowable salt concentrations at different monitoring locations within the specified limits in equations (10) to (15). The Pareto optimal front

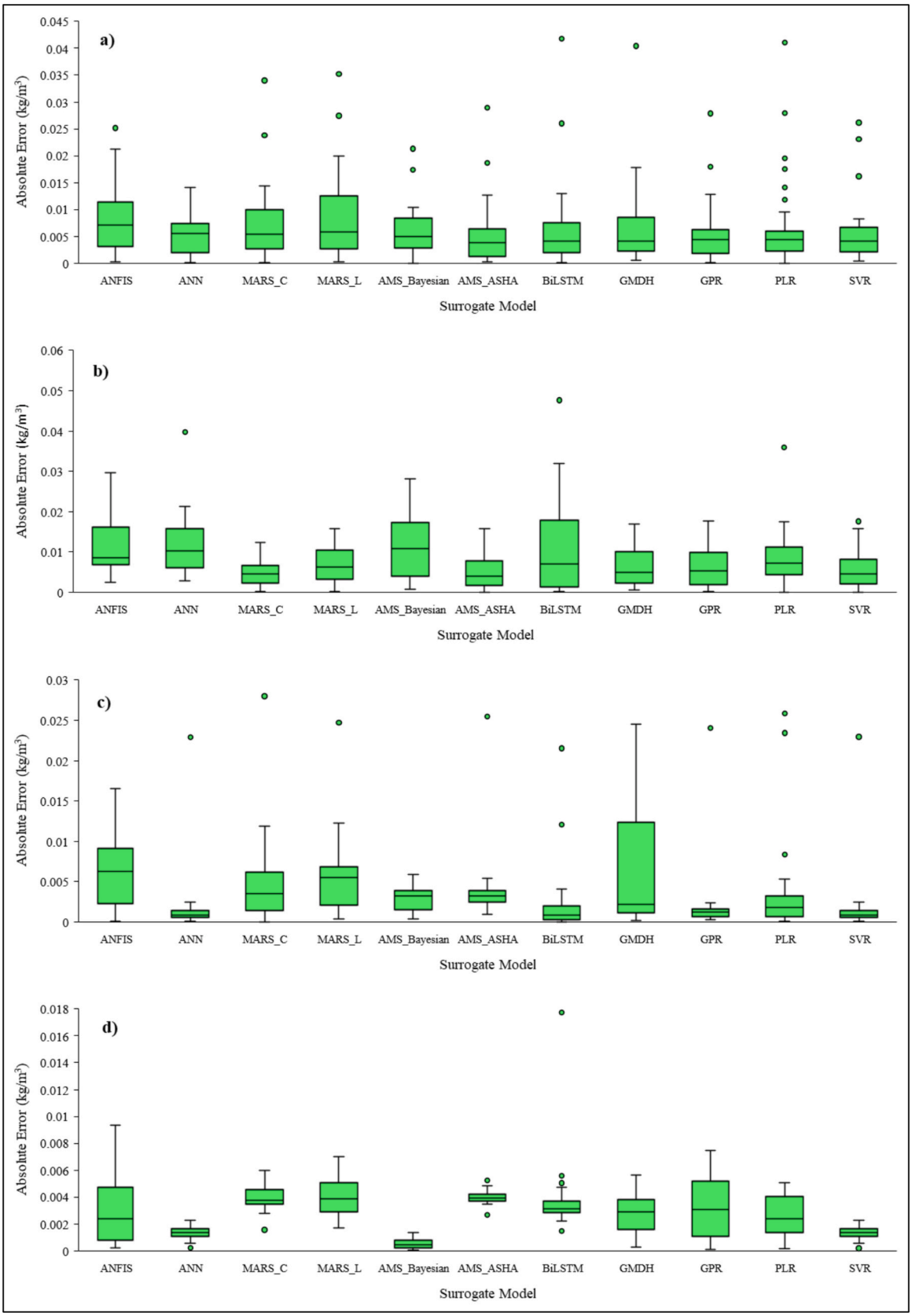


Fig. 6. Boxplots of absolute errors between actual and predicted salt concentration values at **a)** ML1, **b)** ML2, **c)** ML3, and **d)** ML4 using all twelve surrogate models.

Table 4
Entropy weight of performance indices.

Performance Indices	Entropy Weight			
	ML1	ML2	ML3	ML4
R2	0.137	0.144	0.100	0.178
IOA	0.169	0.179	0.132	0.238
KGE	0.151	0.156	0.161	−0.084
MAD	0.181	0.173	0.192	0.218
RMSE	0.181	0.174	0.221	0.231
MAPE (%)	0.181	0.173	0.193	0.218
Sum	1.0	1.0	1.0	1.0

demonstrates the balance between two competing objectives. Its extensive nature indicates that the trade-offs between these objectives are thoroughly represented. Fig. 8 illustrates that 15,000 m^3/d could be extracted from the production bores from Tagabe coastal aquifer with a relatively small amount of barrier well abstraction (253 m^3/d). However, if higher production bore pumping is performed, then higher barrier well pumping would be required to keep the hydraulic gradient towards the seaward side.

A similar method was used by Roy and Datta (2017a; 2017b), Lal and Datta (2018). The authors compared a few surrogate models (less than five) and formed ensembles out of them. In this study, a total of 12 surrogate models were developed and compared. Then, the top-performing 5 surrogate models, determined by Shannon's Entropy based decision theory, were used to form the weighted-average ensemble model. Moreover, other studies (e.g., Bhattacharjya and Datta 2005; Hussain et al. 2015) used a linked S-O technique. However, these authors used single surrogate models that were linked with the optimisation algorithms. Linking multiple surrogates and developing an ensemble reduces the uncertainty in the prediction of salt concentrations (outputs). The ensembles developed in this study performed exceptionally well compared with standalone surrogates.

Table 5
Entropy weight of the individual prediction models.

Standalone models	ML1		ML2		ML3		ML4	
	EW	Rank	EW	Rank	EW	Rank	EW	Rank
ANFIS	0.745	7	0.605	9	0.425	9	0.191	7
ANN	0.918	1	0.436	11	0.915	1	0.598	2
MARS_C	0.697	8	0.994	1	0.423	10	0.151	10
MARS_L	0.572	9	0.820	5	0.300	12	0.125	11
AMS_Bayesian	0.912	2	0.639	8	0.444	7	0.806	1
AMS_ASHA	0.877	5	0.926	2	0.505	6	0.201	6
Bi-LSTM	0.533	11	0.315	12	0.542	5	0.093	12
GMDH	0.508	12	0.815	7	0.351	11	0.172	8
GPR	0.891	4	0.817	6	0.673	4	0.238	5
PLR	0.904	3	0.833	4	0.822	3	0.525	3
RF	0.549	10	0.446	10	0.442	8	0.152	9
SVR	0.816	6	0.865	3	0.840	2	0.341	4

EW = Entropy Weight, ANFIS = Adaptive Neuro Fuzzy Inference System, ANN = Artificial Neural Network, MARS_C = Multivariate Adaptive Regression Spline with Piecewise Cubic Spline, MARS_L = Multivariate Adaptive Regression Spline with Piecewise Linear Spline, AMS_Bayesian = Bayesian Optimization tuned Automatic Model Selection, AMS_ASHA = Asynchronous Successive Halving Algorithm tuned Automatic Model Selection, Bi-LSTM = Bi-directional Long Short term Memory Network, GMDH = Group Method of Data Handling, GPR = Gaussian Process Regression, PLR = Probabilistic Linear Regression, SVR = Support Vector Regression.

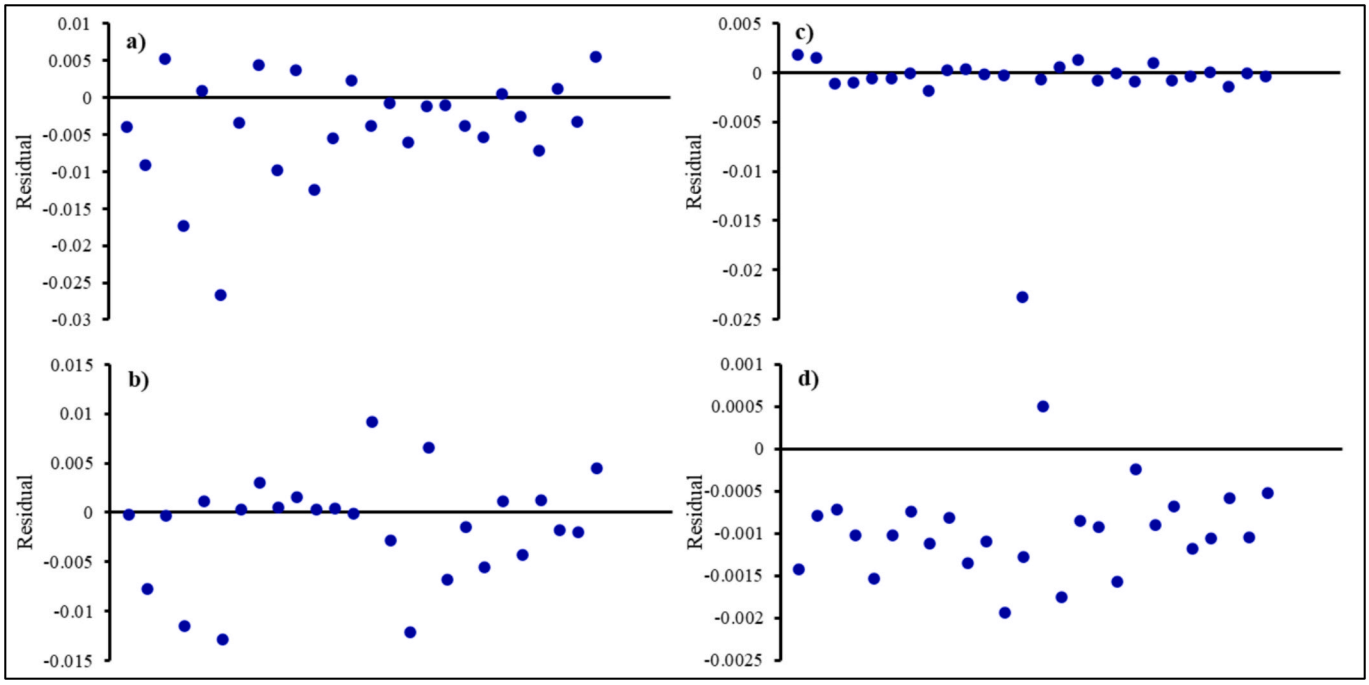


Fig. 7. Residual of actual versus predicted salt concentrations of ensemble models. **a)** residual of an ensemble model at ML1, **b)** residual of an ensemble model at ML2, **c)** residual of an ensemble model at ML3 and **d)** residual of an ensemble model at ML4.

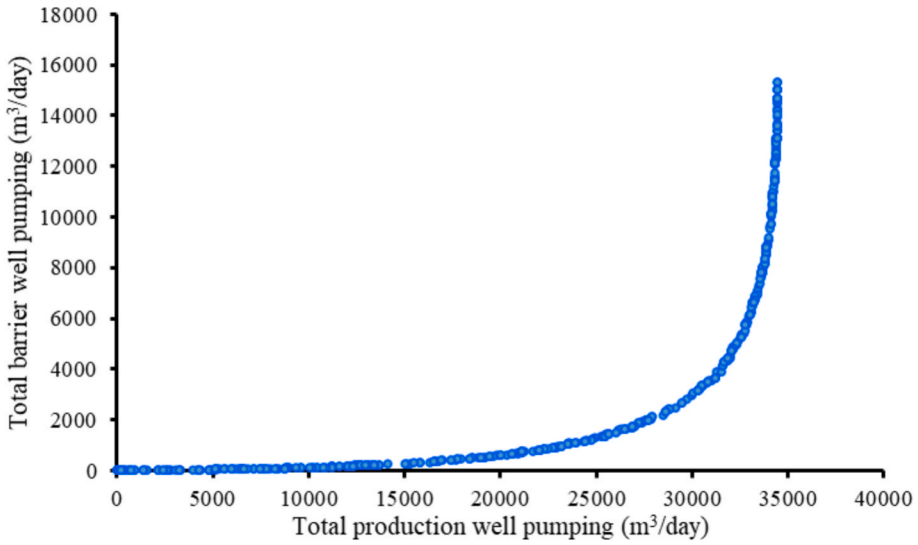


Fig. 8. Pareto optimal front of the linked simulation-optimisation management model.

3.5. Validation of Pareto optimal solutions

The effectiveness of the surrogate-based saltwater intrusion management model was assessed by checking how well it met the specified constraints. The results showed that the saltwater concentrations from the optimisation model, which used surrogate models, consistently stayed below the set maximum allowable levels at all monitoring sites. This indicates that the constraints were fully satisfied without any breaches during the optimisation process. Additionally, the saltwater concentrations closely matched the specified limits, suggesting that the optimisation model effectively converged near the upper limits of the constraints.

The Pareto optimal solutions obtained using the ensemble-CEMOGA optimisation models at respective MLs were verified and validated. Five randomly selected optimal solutions (pumping values) were fed into the SEAWAT-based numerical groundwater model, and the outputs (salt concentrations) of the numerical model were compared with the salt concentrations prespecified by the linked S-O model. The validation results are given in Table 6. The results (Table 6) indicated that the relative error (RE) between the simulated and predicted salt concentrations at four MLs ranged between 0.47% and 6.66%. The salinity concentrations of both models had a minimal difference (RE $<$ 7%), which indicated that the optimal solutions converged to the upper limit of the constraints. Also, it can be reported that all the constraints are satisfied with no constraint violations. The findings in this study are similar to the results reported by Roy and Datta (2017b). The authors suggested that relative errors of less than 10% are considered appropriate and effective for developing an optimal management strategy using an integrated S–O approach. Hence, it could be stated that the machine learning-based ensemble model developed could be replaced with the complex nonlinear coupled density-dependent SEAWAT-based model for developing optimal groundwater management solutions for Tagabe coastal aquifer. Moreover, this methodology could be utilised for other aquifers.

The limitation of this study was the number of data sets used to train and test the surrogate models. The current study used 130 sets of input–output data from the numerical model to train and test the surrogate models. Hence, some of the deep learning models did not perform that well when compared with the machine learning models. Also, larger datasets will be used to train and test the deep learning models in future.

4. Conclusion

Saltwater intrusion is a concern in Vanuatu for Tagabe coastal aquifer based on current groundwater pumping regimes. To manage the saltwater intrusion, optimal management strategies need to be developed. The current study developed a methodology using a linked simulation-optimisation (S-O) technique that provided optimal management strategies of managing saltwater intrusion in Tagabe coastal aquifer. S-O methodology was developed using an ensemble surrogate modelling approach where twelve surrogate models were trained with the input–output patterns from the SEAWAT-based numerical simulation model. Using the Shannon's entropy weight (decision theory), top five surrogates were ranked and selected to form an ensemble model for each monitoring location. All the ensemble models performed exceptionally well compared with standalone surrogates. Later, the ensemble models were externally linked in MATLAB with the Controlled Elitist Multiple Objective Genetic Algorithm (CEMOGA) to optimise the saltwater intrusion management solutions.

The constraints fixed for the S-O model were maximising the

Table 6
Validation of Pareto optimal front solutions with the numerical simulation model.

Solution Number	ML1			ML2			ML3			ML4		
	NSM (kg/m^3)	ESM (kg/m^3)	RE (%)	NSM (kg/m^3)	ESM (kg/m^3)	RE (%)	NSM (kg/m^3)	ESM (kg/m^3)	RE (%)	NSM (kg/m^3)	ESM (kg/m^3)	RE (%)
1	0.320	0.301	6.547	0.282	0.300	5.930	0.299	0.300	0.481	0.314	0.300	4.814
2	0.312	0.300	3.783	0.283	0.300	5.721	0.299	0.300	0.473	0.285	0.300	5.157
3	0.313	0.304	2.916	0.290	0.300	3.237	0.299	0.301	0.658	0.311	0.300	3.525
4	0.321	0.301	6.658	0.282	0.300	5.886	0.299	0.300	0.485	0.314	0.300	4.734
5	0.320	0.301	6.407	0.283	0.300	5.509	0.299	0.300	0.443	0.294	0.300	2.065

NSM – Numerical simulation model; ESM = ensemble surrogate model; RE = absolute relative error between the simulated and the predicted salt concentrations; ML = Monitoring location; C = Concentration

pumping from the production wells, minimising the pumping from the barrier well, and maintaining the maximum allowable salt concentrations at each monitoring location. Conflicting constraints were easily solved with the S-O methodology developed in this study. The S-O model gave Pareto optimal front solutions, maximising the pumping from production wells and minimising the pumping from barrier wells. To verify the Pareto optimal solutions, five random pumping values (Pareto solutions) were fed into the numerical simulation model, and the same was fed into the surrogate ensemble model. The results indicated that the salt concentrations (outputs) from both models had a minimal relative error of less than 7%, satisfying the constraints.

In addition, the results from this study indicated that the use of machine learning in groundwater modelling is a robust tool for predicting the saltwater intrusion in Tagabe coastal aquifer. The use of surrogate ensemble models reduced the computational burden and exertions faced during the optimisation stage. The results also indicated that training different machine learning surrogates with limited datasets was also successful. The S-O management model also proved to be robust in generating optimal solutions for managing the saltwater intrusion in Tagabe coastal aquifer. The methodology proposed in this study is of global significance and can be used by policymakers and water monitoring authorities to draw up policies and regulations for groundwater use in Vanuatu. The methodology presented in this study could also be used in other coastal aquifers to manage saltwater intrusion and conserve groundwater.

The future scope of work has also been planned for Tagabe coastal aquifer, where other constraints would be considered in the S-O methodology to manage SWI. For instance, minimising the recharge, maximising the evapotranspiration and salt concentrations at monitoring locations, using other optimising algorithms and using larger input–output data sets in training and testing surrogate and ensemble models.

CRediT authorship contribution statement

Ashneel Sharan: . **Dilip Kumar Roy:** Writing – review & editing, Supervision. **Bithin Datta:** Writing – review & editing, Supervision, Conceptualization. **Alvin Lal:** Writing – review & editing, Supervision.

Funding

Not applicable.

Declaration of competing interest

The authors declare that they have no known competing financial interests or personal relationships that could have appeared to influence the work reported in this paper.

Acknowledgements

The authors are grateful to Erie Sami from the Department of Water Resources, Government of Vanuatu, for his support in providing valuable groundwater data and timely discussions.

Ethics approval and consent to participate

Not applicable.

Consent for publication

All authors agree to publish.

Appendix A. Supplementary data

Supplementary data to this article can be found online at https://doi.org/10.1016/j.jhydrol.2026.135128.

Data availability

Data will be made available on request.

References

Abdoulhalik, A., Ahmed, A., Hamill, G.A., 2017. A new physical barrier system for seawater intrusion control. J. Hydrol. 549, 416–427. https://doi.org/10.1016/j.jhydrol.2017.04.005.

Ahmed, S.F., Alam, M.S.B., Hassan, M., Rozbu, M.R., Ishtiak, T., Rafa, M., Mofijur, M., Ali, A.M.B.S., Gandomi, A.H., 2023. Deep learning modelling techniques: current progress, applications, advantages, and challenges. Artif. Intell. Rev. 56, 13521–13617. https://doi.org/10.1007/s10462-023-10466-8.

Bath, A.H., Burgess, W.G., Carney, J.N., 1986. The chemistry and hydrology of thermal springs on Efate, Vanuatu. SW Pacific. Geothermics 15 (3), 277–294.

Bhattacharjya, R.K., Datta, B., 2005. Optimal management of coastal aquifers using linked simulation optimization approach. Water Resour. Manag. 19, 293–320. https://doi.org/10.1007/s11269-005-3180-9.

Bhattacharjya, R.K., Datta, B., Satish, M.G., 2007. Artificial neural networks approximation of density dependent saltwater intrusion process in coastal aquifers. J. Hydrol. Eng. 12 (3), 273. https://doi.org/10.1061/(ASCE)1084-0699(2007)12.

Bishop, C.M., 2006. Pattern Recognition and Machine Learning. Springer.

Breiman, L., 2001. Random forests. Mach. Learn. 45 (1), 5–32. https://doi.org/10.1023/A:1010933404324.

Brownlee J (2019) What is deep learning? Machine Learning Mastery. Accessed online on 03/06/2024. Accessed from https://machinelearningmastery.com/what-is-deep-learning/.

CRCP (2021) Report on Climate Risk Country Profile (CRCP): Vanuatu (2021): The World Bank Group. chrome-extension://efaidnbmnnnibpcajpcglclefindmkaj/https://climateknowledgeportal.worldbank.org/sites/default/files/country-profiles/15825-WB_Vanuatu%20Country%20Profile-WEB.pdf.

Datta, B., Peralta, R.C., 1986. Interactive computer graphics-based multi-objective decision-making for regional groundwater management. Agric. Water Manag. 11 (2), 91–116.

Deb K, Goel T (2001) Controlled Elitist Non-dominated Sorting Genetic Algorithms for Better Convergence. In: Zitzler, E., Thiele, L., Deb, K., Coello Coello, C.A., Corne, D. (eds) Evolutionary Multi-Criterion Optimization. EMO 2001. Lecture Notes in Computer Science, vol 1993. Springer, Berlin, Heidelberg. https://doi.org/10.1007/3-540-44719-9_5.

Dhar, A., Datta, B., 2009. Saltwater intrusion management of coastal aquifers. I: Linked simulation-optimisation. J. Hydrol. Eng. 14 (12), 1263–1272. https://doi.org/10.1061/(ASCE)HE.1943-5584.0000097.

Dou, T., Lopes, Y.K., Rockett, P., Hatchway, E.A., Saber, E., 2020. Model predictive control of non-domestic heating using genetic programming dynamic models. Appl. Soft Comput. J. 97 (Part B). https://doi.org/10.1016/j.asoc.2020.106695.

Friedman, J.H., 1991. Multivariate adaptive regression splines. Ann. Stat. 19 (1), 1–67. https://doi.org/10.1214/aos/1176347963.

Gelman, A., Carlin, J.B., Stern, H.S., Dunson, D.B., Vehtari, A., Rubin, D.B., 2013. Bayesian Data Analysis, 3rd ed. CRC Press.

Guo W, Langevin CD (2002) User's Guide to SEAWAT: A computer program for simulation of three-dimensional variable density groundwater flow. *Techniques of water-resources investigations of the US Geological Survey*, book 6, Chapter A7.

Halton, J.H., 1960. On the efficiency of certain quasi-random sequences of points in evaluating multi-dimensional integrals. Numer. Math. 2 (1), 84–90. https://doi.org/10.1007/bf01386213.

Hochreiter, S., Schmidhuber, J., 1997. Long short-term memory. Neural Comput. 9 (8), 1735–1780.

Hussain, M.S., Javadi, A.A., Ahangar-Asr, A., Farmani, R., 2015. A surrogate model for simulation–optimisation of aquifer systems subjected to seawater intrusion. J. Hydrol. 523. https://doi.org/10.1016/j.jhydrol.2015.01.079.

Ivakhnenko, A.G., 1968. The group method of data handling-arrival of the method of stochastic approximation. Soviet Automatic Control 13 (3), 43–55.

Jang, J.S.R., 1993. ANFIS: adaptive-network-based fuzzy inference system. IEEE Trans. Syst. Man Cybern. 23 (3), 665–685.

Kopsiaftis, G., Protopapadakis, E., Voulodimos, A., Doulamis, N., Mantoglou, A., 2019. Gaussian process regression tuned by Bayesian optimisation for seawater intrusion prediction. Comput. Intell. Neurosci. https://doi.org/10.1155/2019/2859429.

Koza, J.R., 1992. Genetic Programming: On the Programming of Computers by Means of Natural Selection; MIT Press: Cambridge, MA, USA, 1992; Volume 1.

Kumar, D.S., 2013. Artificial Neural Networks in Geotechnical Engineering: Modeling and Application Issues. *Metaheuristics in Water, Geotechnical and Transport Engineering*. Elsevier, London, ISBN: 978-0-12-398296-4, Page 231-270.

Lal, A., Datta, B., 2018. Development and implementation of support vector machine regression surrogate models for predicting groundwater pumping-induced saltwater intrusion into coastal aquifers. Water Resour. Manag. 32 (7), 2405–2419. https://doi.org/10.1007/s11269-018-1936-2.

Lal, A., Datta, B., 2020. Application of the group method of data handling and variable importance analysis for prediction and modelling of saltwater intrusion processes in coastal aquifers. Neural Comput. Appl. https://doi.org/10.1007/s00521-020-05232-.

Li, X., Wang, K., Liu, L., Xin, J., Yang, H., Gao, C., 2011. Application of the entropy weight and TOPSIS method in safety evaluation of coal mines. Procedia Eng. 26, 2085–2091. https://doi.org/10.1016/j.proeng.2011.11.2410.

Mo, S., Zabaras, N., Shi, X., Wu, J., 2020. Integration of adversarial autoencoders with residual dense convolutional networks for estimation of non-Gaussian hydraulic conductivities. Water Resour. Res. 56 (2), e2019WR026082.

Papadopoulou, M.P., Nikolos, I.K., Karatzas, G.P., 2010. Computational benefits using artificial intelligent methodologies for the solution of an environmental design problem: saltwater intrusion. Water Sci. Technol. 62 (7), 1479–1490. https://doi.org/10.2166/wst.2010.442.

Parveen, N., Zaidi, S., Danish, M., 2016. Support vector regression model for predicting the sorption capacity of lead (II). Perspect. Sci. 8, 629–631.

Rogers, L.L., Dowla, F.U., Johnson, V.M., 1995. Optimal field-scale groundwater remediation using neural networks and the genetic algorithm. Environ. Sci. Technol. 29 (5), 1145–1155. https://doi.org/10.1021/es00005a003.

Roy, D.K., Datta, B., 2017a. A surrogate based multi-objective management model to control saltwater intrusion in multi-layered coastal aquifer systems. Civ. Eng. Environ. Syst. 34 (3–4), 238–263. https://doi.org/10.1080/10286608.2018.1431777.

Roy, D.K., Paul, C.R., Munmun, T.H., 2024. Datta B (2024) an automatic model selection-based machine learning approach to predict seawater intrusion into coastal aquifers. Environ. Earth Sci. 83, 287. https://doi.org/10.1007/s12665-024-11589-z.

Roy, D.K., Datta, B., 2017b. Multivariate adaptive regression spline ensembles for management of multilayered coastal aquifers. J. Hydrol. Eng. 22 (9). https://doi.org/10.1061/(ASCE)HE.1943-5584.0001550.

Roy, D.K., Datta, B., 2020. Modelling and management of saltwater intrusion in a coastal aquifer system: a regional-scale study. Groundw. Sustain. Dev. 11. https://doi.org/10.1016/j.gsd.2020.100479.

Roy, D.K., Lal, A., Sarker, K.K., Saha, K.K., Datta, B., 2021. Optimisation algorithms as training approaches for prediction of reference evapotranspiration using adaptive neuro fuzzy inference system. Agric Water Manag 255. https://doi.org/10.1016/j.agwat.2021.107003.

Salford Predictive Modeler, 2019. Introducing MARS: Multivariate adaptive regression spline, Minitab. 1-35. https://www.minitab.com/content/dam/www/en/uploadedfiles/content/products/spm/IntroMARS.pdf.

Shannon, C.E., 1948. A mathematical theory of communication. Bell Syst. Tech. J. 27, 379–423. https://doi.org/10.1002/j.1538-7305.1948.tb01338.x.

Sharan, A., 2023. Analysing the effects of tropical cyclone on critical frequency of the F 2-Region Ionosphere in South Pacific Region. Geomag. Aeron. 62 (Suppl 1), S128–S141. https://doi.org/10.1134/S0016793222600175.

Sharan, A., Datta, B., Lal, A., 2023. Integrating numerical modelling and scenario-based sensitivity analysis for saltwater intrusion management: case study of a complex heterogeneous island aquifer system. Environ. Monit. Assess. 195 (5), 553. https://doi.org/10.1007/s10661-023-11159-z.

Sharan, A., Datta, B., Lal, A., 2024. Management of saltwater intrusion using 3D numerical modelling: a first for Pacific Island country of Vanuatu. Environ. Monit. Assess. 196 (120). https://doi.org/10.1007/s10661-023-12245-y.

Sharan, A., Lal, A., Datta, B., 2021. A review of groundwater sustainability crisis in the Pacific Island countries: challenges and solutions. J. Hydrol. 603, 1–15. https://doi.org/10.1016/j.jhydrol.2021.127165.

Sherif, M., Sefelnasr, A., Ebraheem, A.A., Javadi, A., 2014. Quantitative and qualitative assessment of seawater intrusion in wadi ham under different pumping scenarios. J. Hydrol. Eng. 19 (5), 855–866. https://doi.org/10.1061/(ASCE)HE.1943-5584.0000907.

Snoek J, Larochelle H, Adams RP (2012) Practical Bayesian Optimization of Machine Learning Algorithms. *In Advances in Neural Information Processing Systems*, pp. 2951-2959.

Song, J., Yang, Y., Wu, J., Wu, J., Sun, X., Lin, J., 2018. Adaptive surrogate model based multi-objective optimisation for coastal aquifer management. J. Hydrol. 561, 98–111. https://doi.org/10.1016/j.jhydrol.2018.03.063.

Sreekanth, J., Datta, B., 2011. Coupled simulation-optimisation model for coastal aquifer management using genetic programming-based ensemble surrogate models and multiple-realisation optimisation. Water Resour. Res. 47 (4). https://doi.org/10.1029/2010WR009683.

Tenne, Y., Goh, C.K., 2010. Computational Intelligence in Expensive Optimisation Problems. Springer-Verlag, Berlin Heidelberg.

TRCMP (2018) Tagabe River Catchment Management Plan (TRCMP) 2017- 2030. Report by Tagabe River Management Committee. Retrieved from https://www.pacific-r2r.org/sites/default/files/2020-03/Tagabe%20River%20Management%20Plan%20%282017-2030%29.pdf.

UNDP (2016) State of the Environment Report for Port Vila, Vanuatu. Report from United Nations Development Programme (UNDP). Retrieved from https://www.vu.undp.org/content/vanuatu/en/home/library/environment_energy/State_of_Environment_Report_2016.html.

VGO (2015) Port Vila urban geohazard assessment. Report from Vanuatu Geohazards Observatory (VGO). Retrieved from http://www.vmgd.gov.vu/vmgd/images/stories/Publications/Reports/Port%20Vila%20Urban%20Geohazard%20Assessment%20Report.pdf.

VMGD (2023) Vanuatu Meteorology & Geohazards Department (VMGD). Retrieved from https://www.vmgd.gov.vu/vmgd/index.php/forecast-division/tropical-cyclone.

Wang, Y.M., Chin, K.S., Poon, G.K., 2007. Entropy weighting based decision making in multicriteria fuzzy systems. Int. J. Approx. Reason. 44 (2), 124–140.

WTTC (2021). Vanuatu: Travel & Tourism Economic Impact 2021. Retrieved from https://wttc.org/Research/Economic-Impact/Country-Analysis-Reports.

Yang, T., Feng, B., Chien, J., Krishnan, S., Agrawal, G., 2019. AdaFLO: Adaptive Fuzzy Linear Optimization for Online Hyperparameter Tuning. In: In Proceedings of the 2019 *SIAM International Conference on Data Mining (SDM)*, pp. 221–229.